Towards the Visualisation of the Turbulence Cascade

M. Mascini

Technische Universiteit Delft

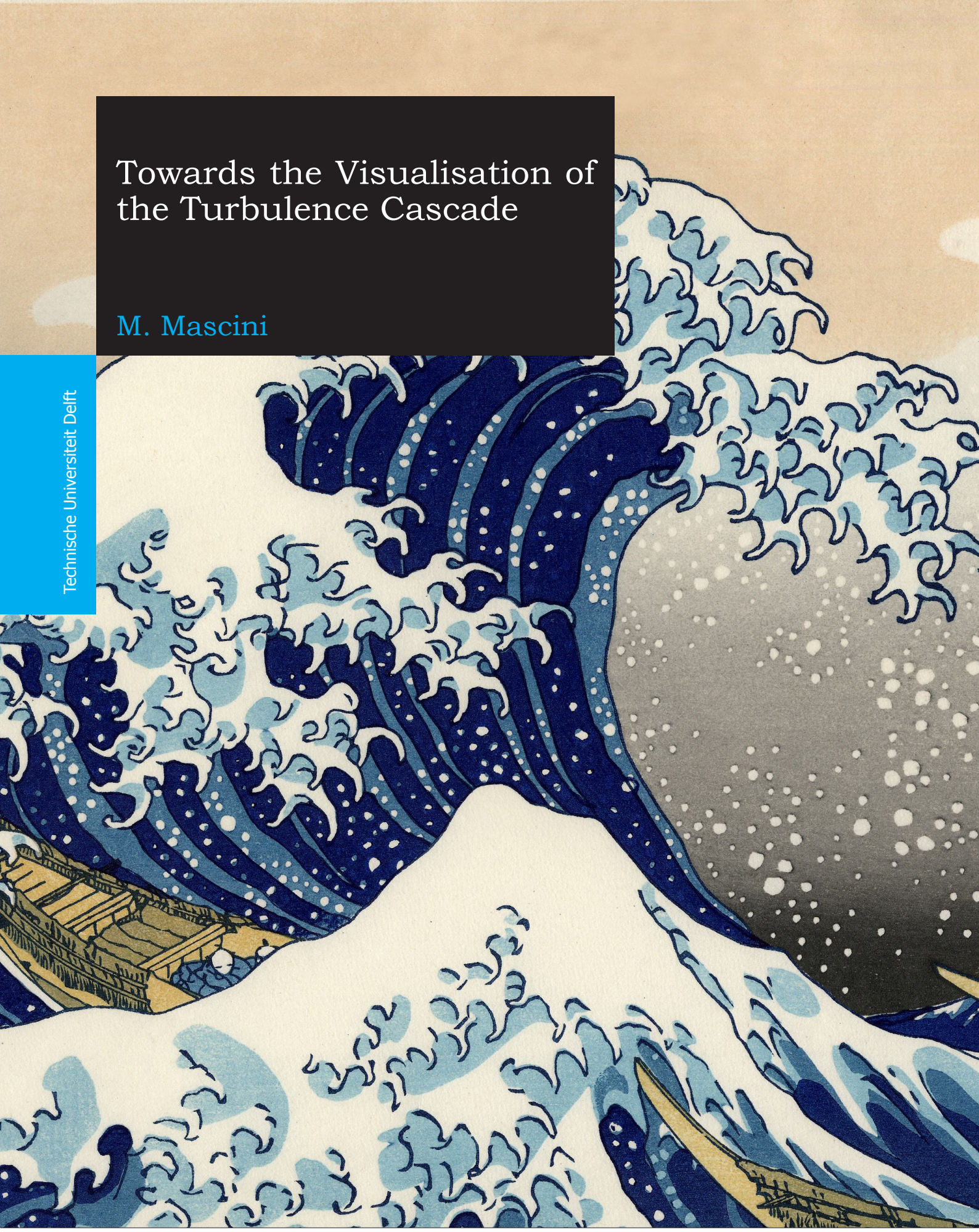

TU Delft Delft University of Technology

Challenge the future

TOWARDS THE VISUALISATION OF THE TURBULENCE CASCADE

by

M. Mascini

in partial fulfillment of the requirements for the degree of

Bachelor of Science
in Molecular Science and Technology

at the Delft University of Technology,
to be defended publicly on Friday the 6th of July 2018, at 11:00.

Student number:	4393333
Supervisor:	Ir. S. Mukherjee
Thesis committee:	Dr. L. Portela
	Dr. S. Kenjereš

Cover image: Katsushika Hokusai — *The Great Wave off Kanagawa*,
courtesy of the British Museum, London.

An electronic version of this thesis is available at http://repository.tudelft.nl/.

TU Delft Delft University of Technology

ABSTRACT

A turbulent flow is composed of swirling eddies of many sizes. Energy, which is added to the flow at the larger scales, is transferred down through consecutively smaller eddies until the scale is small enough that viscous forces dominate, at which point the energy is dissipated [1]. The mechanism by which energy is transferred down the scales of eddies is generally described as eddy break-up, but the process of eddies breaking into smaller eddies has never been directly observed. The objective of this research is to identify and visualize eddies and their breakage into smaller eddies in numerically simulated isotropic turbulence flows. A correlation vector is defined at each point in space, based upon the dot product of velocity over spatial distance. This function shows eddies as the result of correlation over the entire field for each point, in contrast to earlier eddy identification techniques which focus only on local properties of the flow, such as kinetic energy magnitude [2]. The resultant correlation field shows blobs of high correlation, which can be interpreted as the kernel of a coherent structure in the flow. These kernels can be seen splitting into smaller kernels over time — an indication of the turbulent energy cascade at work. Making use of the Biot-Savart law, the velocity field associated with a coherent blob of correlation is generated from the associated vorticity field. The reconstructed velocity field is vortex-like in structure, and appears to break into two separate vortices as the kernel separates into two distinct kernels, yielding a visualization of turbulent eddy dynamics in real space — the first step towards the visualization of the turbulent energy cascade.

CONTENTS

1

INTRODUCTION

Most flows around you are turbulent. Consider the mixing of milk into your coffee, the flow of air above a candle, the foaming mess at a waterfall's base; turbulence is everywhere. Being able to accurately describe these flows, and being able to predict how they will develop, is an active area of research. Advancements in this field give rise to advancements in industrial chemical engineering, medicine, weather prediction, geophysics and many other areas to which the modelling of turbulent flows is integral.

In addition to its use in furthering scientific knowledge in the above-mentioned fields, research into turbulent flows is motivated simply by its enigma. The elegant patterns inherent to turbulence, whose complex behaviour arises from 'simple' laws, should in and of itself be reason enough to warrant further research. With this beauty come other benefits: staring into the turbulent flames of a campfire reduces blood pressure[3], and it has been theorized that the act of gathering around a fire at night is what led to the development of singing, dancing, storytelling and many other foundations of culture[4]. Thus form and function are interlinked even in fluid mechanics.

This bachelor thesis is aimed towards visualizing one aspect of turbulent flows, namely the turbulent energy cascade. Lewis Fry Richardson described this process quite poetically:

> *"Big whirls have little whirls, which feed on their velocity,*
> *And little whirls have lesser whirls, and so on to viscosity"*

Richardson was an English poly-scientist whose name is attached to many techniques and ideas in mathematics, physics, and meteorology. His poem refers to the process by which energy is transferred and eventually dissipated in all turbulent flows[1]. The fact that energy is indeed transferred across scales and dissipated at the smallest scales is undisputed. However, the break-up of large eddies into smaller eddies has not yet been adequately described or visualized.

In this project, a new method of identifying turbulent eddies by spatially isolating them as regions of highly coherent motion is proposed. Earlier attempts at visualizing eddies considered an eddy to be a contour of high turbulent energy. This approach is bound by its locality; it says nothing about the patterns and structures found elsewhere in the flow. The proposed method of this project considers eddies as a finite region with a certain coherent structure. By considering the instantaneous correlation for each point in the field, a spatial correlation vector field is defined, which contains information about structures on a non-local scale.

It is found that considering eddies in this manner leads to well-defined blobs within the correlation field that appear, merge, split and disappear. These blobs can be seen as the kernels of larger coherent structures. The velocity field associated with these kernels can be generated by making use of Biot-Savart's law. The velocity fields generated in this way show vortex-like structures, which appear to move as the kernel breaks into two distinct kernels. These results are promising and may lead to new insights on the possibilities of characterizing vortical motions by bridging point concepts to non-local coherent structures, and with that eventually the visualization of the turbulent energy cascade.

[1] Whether or not there exists a universal theory of turbulence, justifying statements such as 'all turbulent flows', has been neither proved nor disproved[5], and is an entirely different but equally interesting question, which for obvious reasons this project will not even attempt to tackle.

2

THEORY

Investigating the turbulent energy cascade requires some groundwork in fluid mechanics. For this, a number of books have been indispensable [6–8]. Throughout this project, the fluid being investigated is an incompressible Newtonian fluid. For a full derivation of some of the more important equations described below, see appendix A.

2.1. THE EQUATIONS OF MOTION

Instead of investigating the motion of single molecules, the statistical average velocity $\mathbf{u}(\mathbf{x}, t)$ of the fluid is used[2]. This approach is valid as long as the size of the system under investigation is of a much larger scale than the size of the motion of the individual molecules.

2.1.1. CONSERVATION OF MASS: THE CONTINUITY EQUATION

By considering a small differential control volume within a flowing liquid, and setting up a mass balance over this volume, one arrives at:

$$\frac{\partial \rho}{\partial t} + \nabla \cdot (\rho \mathbf{u}) = 0. \tag{2.1}$$

Since the fluid is incompressible, this equation reduces to

$$\nabla \cdot \mathbf{u} = 0. \tag{2.2}$$

This is the continuity equation. It implies that the divergence of $\mathbf{u}$ is zero everywhere; whatever amount of fluid flows into an arbitrary control volume must also be flowing simultaneously out of it.

2.1.2. CONSERVATION OF MOMENTUM: THE NAVIER-STOKES EQUATION

The Navier-Stokes equations describe the motion of a fluid. To derive them, Newton's second law of motion is applied to a small volume of fluid δV, upon which all surface and body forces are considered, yielding

$$\frac{D\mathbf{u}}{Dt} = \mathbf{g} - \nabla\left(\frac{p}{\rho}\right) + \nu \nabla^2 \mathbf{u}. \tag{2.3}$$

Here the notation $\frac{D}{Dt}$ is used for the material derivative, which is the derivative for a travelling control volume (see chapter A.2 for a derivation of the material derivative). This seems like a rather common partial differential equation, not unlike the wave equation or the diffusion equation. However, liquids flowing according to the Navier-Stokes equation display chaotic[3] results, instabilities and turbulence, which is true for neither the wave nor the diffusion equation. To see why this is, the material derivative is expanded:

$$\frac{\partial \mathbf{u}}{\partial t} + \mathbf{u} \cdot \nabla \mathbf{u} = \mathbf{g} - \nabla\left(\frac{p}{\rho}\right) + \nu \nabla^2 \mathbf{u}. \tag{2.4}$$

[2] Throughout this report, the vector $\mathbf{u}$ will be used for the velocity, having components u_x, u_y and u_z for the x, y and z component of space, the vector $\mathbf{x} = [x\, y\, z]^T$ denoting space. In other literature, one might find the usage of u, v and w for the three components of velocity.

[3] 'Chaotic' in this context means extreme sensitivity to initial conditions.

The non-linear term $\mathbf{u}\cdot\nabla\mathbf{u}$, which was hidden in the material derivative, is responsible for the chaos inherent to fluid flow. Expanding the material derivative gives another insight: by making use of the solenoidal property of an incompressible fluid ($\nabla\cdot\mathbf{u}=0$) and the Biot-Savart law, an expression for p in terms of $\mathbf{u}$ can be found [7, chap. 2.2]. In this way, equation 2.4 can be rewritten to a deterministic partial differential equation dependent only on $\mathbf{u}$:

$$\frac{\partial\mathbf{u}}{\partial t}=f(\mathbf{u}). \tag{2.5}$$

For a given initial condition, it is theoretically possible to integrate forward in time to find $\mathbf{u}$ at any time and place. Unfortunately, this is computationally expensive, even on modern computers, due to the massive difference in scales present in most turbulent flows. Aside from the cost involved, such a computation serves little purpose, as one is generally more interested in the statistical properties of a point in the flow than in the specific value for $\mathbf{u}$. Luckily, there exist several ways to approximate a solution of the Navier-Stokes equation which are not as computationally expensive.

The terms of equation 2.4 merit some closer examination. On the left hand side is the rate of change of the velocity field over time, and the (nonlinear) advection of velocity. Then, on the right hand side, there is the effect of gravity, the effect of the pressure gradient and the viscuous diffusion of velocity. The non-dimensional form of the Navier-Stokes equation can be found by substituting the relevant scales and dimensionless variables, leading to

$$\frac{\partial\mathbf{u}^*}{\partial t^*}=\frac{1}{Fr^2}\mathbf{g}^*-\nabla^* p^*+\frac{1}{Re}\nabla^{*2}\mathbf{u}^*-\mathbf{u}^*\cdot\nabla^*\mathbf{u}^*. \tag{2.6}$$

Here Fr is the Froude number, which for this project is not relevant, as gravity will be left out of consideration. The Reynolds number Re, however, is very important, as it characterizes whether or not a given flow is prone to become turbulent. From the dimensionless form of the Navier-Stokes equation, it can be seen that the effect of viscous forces is inversely proportional to the Reynolds number. At low Re, viscous effects dominate, but at higher Re the effect of viscosity is negligible compared to nonlinear advection and the pressure gradient.

2.2. VORTICITY

Closely linked to the velocity is the vorticity $\boldsymbol{\omega}$. The vorticity is defined as the curl of the velocity, i.e. $\boldsymbol{\omega}=\nabla\times\mathbf{u}$. It describes the local spinning motion of the fluid. Imagine a tiny volume in the flow suddenly becoming a solid chunk. If the chunk begins rotating about its centre of mass, that area of the flow has vorticity. If however the chunk is simply moving around but not rotating, there is no vorticity. Note that this has nothing to do with the global rotation of the fluid. A whirlpool where the velocity is inversely proportional with the distance from the centre, also known as an irrotational vortex, has no vorticity, although the total flow is definitely spinning around a point. A shear flow on the other hand, *can* have vorticity (see figure 2.1), as a rigid chunk in the flow will have rotated relative to its original orientation over time.

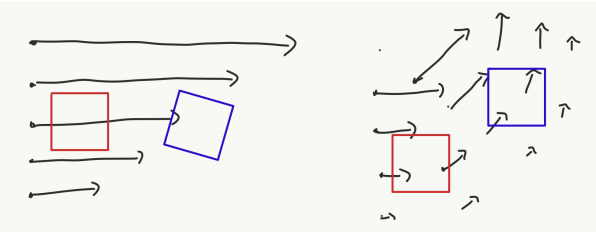

Figure 2.1: A shear flow (left) and an irrotational vortex (right). If the area in the red square becomes solid for a short period of time, then it will end up in the position drawn in blue. The shear flow shows local spinning motion, which is not present in the irrotational flow.

An important result of the Navier-Stokes equations is that they can be used to derive the fact that the pressure p is non-local. This is to say that an eddy at a certain point $\mathbf{x}$ produces pressure waves that are felt everywhere in space, which in turn influences the velocity of the flow. Thus velocity is not really localized in space. If initially the flow is nonzero only for a small part of the domain, this would send pressure waves through the entire domain, causing the fluid to start flowing everywhere soon. Vorticity, on the other hand, can only travel by diffusion or advection. Since the vorticity field is also solenoidal, there exist vortex tubes: bundles of vortex lines which must be either closed loops, or end at a physical boundary. An everyday example of this is a smoke ring.

BIOT-SAVART'S LAW

The relationship $\boldsymbol{\omega} = \nabla \times \mathbf{u}$ may be inverted in infinite domains using the Biot-Savart law:

$$\mathbf{u}(\mathbf{x}) = \frac{1}{4\pi} \int_V \frac{\boldsymbol{\omega}(\mathbf{x}') \times \mathbf{r}}{|\mathbf{r}|^3} d\mathbf{x}', \qquad \mathbf{r} = \mathbf{x} - \mathbf{x}'. \tag{2.7}$$

This is very important for this project, as it allows for reconstructing a velocity field from (part of) a vorticity field, hence isolating contributions of local vorticity to larger scale velocity structures.

2.3. TURBULENCE

As Lesieur describes it [9], *"[turbulence] represents extremely different points of view, all of which have in common their complexity, as well as an inability to solve the problem. It is even difficult to agree on what exactly is the problem to be solved"*. Although no precise formal definition of turbulence exists, there is a general consensus that turbulent flows exhibit the following characteristics:

- **Randomness:** Turbulent flows seem irregular, chaotic and unpredictable.
- **Nonlinearity:** Turbulent flows are highly nonlinear, resulting in chaotic behaviour.
- **Diffusivity:** Due to the high rate of mixing, turbulent flows show high rates of diffusion of heat and momentum.
- **Vorticity:** Turbulent flows show many levels of 'spinning structures' at various scales.
- **Self-similarity:** The structures are display a level of self-similarity across space and time scales. Mandelbrot first hypothesised that aspects of turbulent flow could be seen as fractals [10], after which it was shown by Sreenivasan that they could be assigned a fractal dimension [11].

The simple answer to the question of what turbulence is, is that it is a solution of the Navier-Stokes Equations which displays these characteristics. It must be noted, however, that this is not an exhaustive list of characteristics, nor are these unique to turbulent flows. They share causes and effects, and influence each other greatly, such that it is hard to pinpoint where exactly each of them comes from.

In his 1935 paper [12], G.I. Taylor introduced the concept of homogeneous isotropic turbulence. Homogeneity implies that the statistical properties of the flow are invariant under translations, and isotropic implies that the statistical properties are invariant under rotations. This project restricts itself to homogeneous isotropic turbulence for an incompressible fluid.

2.4. THE TURBULENT ENERGY CASCADE

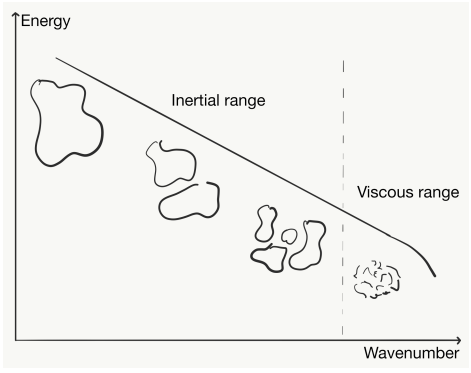

Figure 2.2: The turbulent energy cascade. Energy supplied at the large scale (small wavenumber) is transferred through successively smaller eddies in the inertial range, until it is dissipated at the smallest wavenumbers in the inertial range.

An important characteristic of turbulence is the presence self-similar eddies[4] of many sizes. The largest of these eddies correspond to the scale at which energy is added. These eddies might break up due to inertial forces, from which smaller eddies are generated, which, in turn, might also break up, and so on, until the vortices reach a size where they are more influenced by viscous effects than by inertial effects. It is at this point, when the eddies have a length close to η, the Kolmogorov scale, that energy is dissipated [1] (see figure 2.2).

The reason dissipation happens at the smaller scales only can be found in the Navier-Stokes equations. In equation 2.6, it can be seen that at low Reynolds numbers, viscous effects dominate. The effective Reynolds number of the small scales is also is small, hence viscous effects overcome inertial effects and dissipation occurs.

The usage of the term 'break up' to describe what happens to the large scale eddies is not entirely justified. The actual breaking up of an eddy into two smaller eddies has not been

[4] The term 'eddy' allows no precise definition. For this project, any finite region of coherent motion is considered an eddy.

observed, despite the many drawings similar to figure 2.2 of the process in literature. It is certain that energy is transferred down from the large scales to the smaller scales, at which point it is dissipated, but how this exactly happens is still somewhat of a mystery.

2.5. VISUALISING THE CASCADE BY FOURIER FILTERING

Shortly after Kolmogorov introduced the concept of the turbulent energy cascade, scientists such as Heisenberg [13], Weizsäcker [14] and Onsager [15] started describing the scales in the cascade by the associated wavenumber k. This makes it possible to use the Fourier transform (see chapter A.3) to spectrally filter the velocity field.

Jimenez et al. hypothesize that eddies will manifest in the filtered fields as regions of high kinetic energy [2]. The idea behind the approach is the following; eddies are continuously being formed at the large scale, corresponding to $k = 1$. These eddies break up, transferring energy to smaller scales. By measuring the correlation of energy between scales, a certain temporal delay can be found, from which the eddy lifetime τ can be calculated [16]. At $t = \tau$ the original eddy has broken up into tiny eddies at the Taylor microscale[5] λ, with wavenumber k_λ. Thus it is possible to estimate the wavenumber associated with the original eddy for every timestep between $t = 0$ and $t = \tau$. By filtering out all wavenumbers except the wavenumber associated with the eddy, it can be visualized at each timestep as a region of high kinetic energy.

Figure 2.3 displays the results of this method. This method has two main draw-backs. Firstly, it considers only local properties of the flow, whereas a turbulent eddy has non-local influences on the flow. Secondly, it does not consider the structures present in the flow, but restricts itself to the magnitude of the field. In an attempt to arrive at a better visualization of turbulent eddies, it was decided to investigate eddies as regions of highly coherent flow.

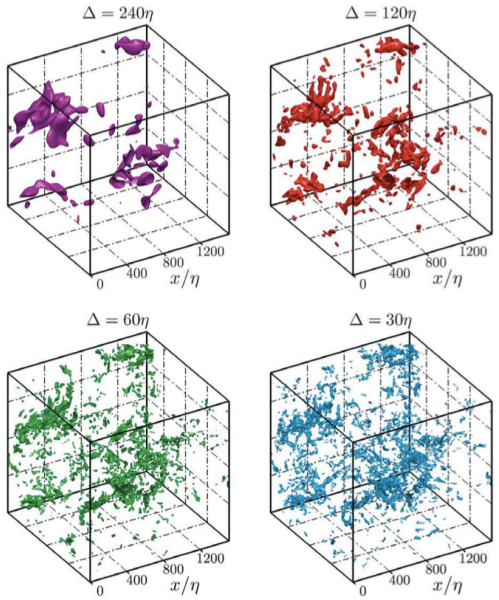

Figure 2.3: Energy eddies at four different scales for a single instance of time, from Jiménez *et al.* [2]

[5] The Taylor microscale, which will be formally introduced in chapter 4, is the length scale at which viscous forces begin to dominate.

3

RESEARCH GOALS

In his 1970 paper [17] surveying the possibilities of a grand theory of turbulence, mathematician Steven Orszag concluded that "*... the principal result of fifty years of turbulence research is the recognition of the profound difficulties of the subject*". This still holds today; although scientists have come a long way since the 1970s by use of powerful computers, there is still much to be discovered.

The turbulent energy cascade, as described by Richardson, accurately characterizes the flow of energy from the larger scales down through the smaller scales until it is dissipated. What the eddies at each scale look like exactly, and how they break up and transfer energy, is currently not known. Many scientific fields would benefit from more knowledge on this subject. With this project, an attempt is made to gain more insight into the eddy structures and the turbulent energy cascade in forced isotropic turbulence flow.

The long-term goal is to visualize the entire turbulent energy cascade, including but not restricted to the shape and structure of an eddy, the eddy break-up mechanism and the manner in which energy is transferred across scales. Richard Feynman once called turbulence "the most important unsolved problem in classical physics". However, in a letter to one of his former students, he had something more to say about which problems are worthwhile, and which are not: *"A problem is grand in science if it lies before us unsolved and we see some way for us to make some headway into it. I would advise you to take even simpler, or as you say, humbler, problems until you find some you can really solve easily, no matter how trivial. You will get the pleasure of success, and of helping your fellow man ... You must not take away from yourself these pleasures because you have some erroneous idea of what is worthwhile"*[18]. With this project, the intention is to follow Feynman's advice and attempt to pragmatically initiate paving the way towards the long-term goal. Concretely, there are two main research questions:

- **How can eddies be described as regions of highly coherent motion in turbulent flow?**
- **How can the velocity fields associated with these eddies be visualized?**

Answering these questions will hopefully make for a better understanding of the turbulent energy cascade, or at least a better understanding of what parts of it are worthwhile to tackle next.

4

DIRECT NUMERICAL SIMULATION OF ISOTROPIC TURBULENCE

Data from two direct numerical simulations of forced isotropic turbulence have been used. The first, which will be referred to from hereon as **flow A**, was simulated at the Transport Phenomena group at TU Delft by Siddhartha Mukherjee. The second was simulated by the John Hopkins Turbulence Database group, and will be referred to as **JHTD**.

4.1. FLOW A

4.1.1. SIMULATION METHOD

Flow A consists of a periodic cube of size 128^3 [nondimensional length units] with 128^3 gridpoints. The periodic cube, while not strictly physical, is often used in turbulence research, as it has many benefits for computational cost and complexity - for example, there are no boundary effects to be taken into consideration. The dataset was generated using the Lattice Boltzmann method, which is second-order accurate in both space and time. The simulation is continuously forced, with a forcing scheme based upon the scheme proposed by Alvelius [19] and ten Cate *et al.* [20], and sharing many features with the forcing scheme used by Perlekar *et al.* [21]. The forcing is calculated in real space using the following formulae:

$$F_x = \sum_{k=k_a}^{k_b} A(k)[\sin(2\pi k y + \phi_y(k)) + \sin(2\pi k z + \phi_z(k))] \tag{4.1}$$

$$F_y = \sum_{k=k_a}^{k_b} A(k)[\sin(2\pi k x + \phi_x(k)) + \sin(2\pi k z + \phi_z(k))] \tag{4.2}$$

$$F_x = \sum_{k=k_a}^{k_b} A(k)[\sin(2\pi k x + \phi_z(x)) + \sin(2\pi k y + \phi_y(k))]. \tag{4.3}$$

Here $\phi_i(k)$ is a random phase for the sine wave in direction i, which causes the forcing to approximate white noise in time. The amplitude A is defined as

$$A(k) = A\exp\left(-\frac{(k-k_f)^2}{c}\right), \tag{4.4}$$

where c is the width over which the force amplitude is to be distributed, and k_f is the central forcing number, which for this simulation was $k_f = 3$. Equation 4.4 is defined in such a way that there exists a dominant wavenumber which contains most of the energy. The summation parameters are $k_a = 1$ and $k_b = 2$.

4.1.2. CHARACTERISTIC FLOW PARAMETERS

The kinematic viscosity of the fluid in flow A is $\nu = 8.4 \times 10^{-4}$ [dimensionless viscosity]. From the simulated velocity, the vorticity $\boldsymbol{\omega}$ and enstrophy $\boldsymbol{\omega}^2$ can be calculated:

$$\boldsymbol{\omega} = \nabla \times \mathbf{u} \tag{4.5}$$

$$\boldsymbol{\omega}^2 = \boldsymbol{\omega} \cdot \boldsymbol{\omega}. \tag{4.6}$$

Using the average enstrophy, the average energy dissipation rate can be calculated:

$$\epsilon = \nu \langle \omega^2 \rangle, \tag{4.7}$$

where the brackets indicate a spatial average.The energy dissipation rate is the amount of energy dissipated per unit volume. From this, the Taylor microscale can be calculated:

$$\lambda = \sqrt{\frac{15\nu}{\epsilon}} \cdot u', \tag{4.8}$$

where u' is the root mean squared velocity. The Taylor microscale is the length scale at which viscous forces begin to dominate. Related to the Taylor microscale is the Taylor-scale Reynolds number

$$Re_\lambda = \frac{u'\lambda}{\nu}. \tag{4.9}$$

The Kolmogorov scale is given as

$$\eta = \left(\frac{\nu^3}{\epsilon}\right)^{\frac{1}{4}}. \tag{4.10}$$

The Taylor-scale Reynolds number is the Reynolds number for the eddies of size λ, and the Kolmogorov scale is the length scale at which energy is dissipated, as outlined by Kolmogorov in his famous paper[1]. The final relevant length scale is the integral length scale L, which gives an indication of the extent of autorrelation in the flow. The autocorrelation for a given point $\mathbf{x}$, direction $\mathbf{e}_i$ (where $\mathbf{e}$ denotes a unit vector) and distance r is defined by

$$f(r) = \frac{\langle \mathbf{u}(\mathbf{x}) \cdot \mathbf{u}(\mathbf{x} + \mathbf{e}_i \cdot r) \rangle}{u'^2}, \tag{4.11}$$

where $\mathbf{u}$ is along $\mathbf{e}_i r$. From this, the integral length can be calculated by taking the integral of $f(r)$ as:

$$L(\mathbf{x}) = \int_0^\infty f(r) dr. \tag{4.12}$$

Alternatively, the integral length scale can be calculated using the relation

$$L = Re_\lambda^{0.75} \eta. \tag{4.13}$$

The large eddy turnover time T_L is found using:

$$T_L = \frac{L}{u'}. \tag{4.14}$$

The values of these parameters in dimensionless units for flow A are:

Domain	$128 \times 128 \times 128$	[length^3]
Viscosity	$\nu = 8.4 \times 10^{-4}$	[length^2/time]
Energy dissipation	$\epsilon = 3.27 \times 10^{-8}$	[energy / (time $\cdot$ mass)]
RMS Velocity	$u' = 0.012$	[length / time]
Taylor microscale	$\lambda = 7.424$	[length]
Taylor-scale Reynolds number	$Re_\lambda = 106$	[-]
Kolmogorov length scale [6]	$\eta = 0.3667$	[length]
Integral length scale	$L = 12.1$	[length]
Large eddy turnover time	$T_L = 1010$	[time]

Figure 4.1 displays a visualisation of the velocity and vorticity profile for flow A.

[6] Here, the Kolmogorov scale is smaller than the grid size, thus the simulation is slightly under-resolved. This potential problem is negated by the fact that there is enough energy dissipation to counter the generation of energy by the forcing, hence the cascade remains well-resolved.

4.2. JHTD FLOW

The John Hopkins Turbulence Database provides datasets of turbulent flows for scientific research. For this project, the 'Forced Isotropic Turbulence Dataset' was used. It is a direct numerical simulation of a 1024^3 periodic cube, where the Navier-Stokes equation is solved using pseudo-spectral method. The relevant dimensionless system parameters are [22]:

Domain	$2\pi \times 2\pi \times 2\pi$	[length^3]
Viscosity	$\nu = 0.000185$	[length^2/time]
Energy dissipation	$\epsilon = 0.103$	[energy / (time $\cdot$ mass)]
RMS Velocity	$u' = 0.686$	[length / time]
Taylor microscale	$\lambda = 0.113$	[length]
Taylor-scale Reynolds number	$Re_\lambda = 418$	[-]
Kolmogorov length scale	$\eta = 0.0028$	[length]
Integral length scale	$L = 1.364$	[length]
Large eddy turnover time	$T_L = 1.99$	[time]

A single timestep of resolution 512^3 was retrieved by coarse-graining the 1024^3 data and used for the eddy identification investigation. Figure 4.2 displays a visualization of the velocity and vorticity profile for JHTD.

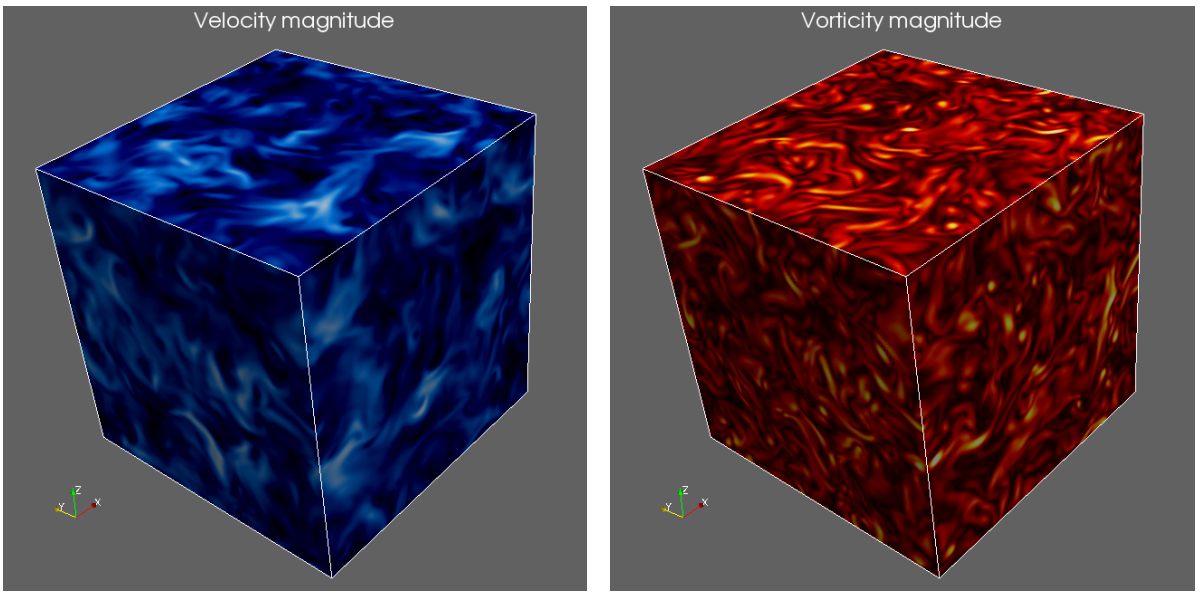

Figure 4.1: Velocity (left) and vorticity (right) magnitude visualisation at t=46000 for flow A. Higher magnitudes are represented by a lighter colour, lower magnitudes by a darker colour.

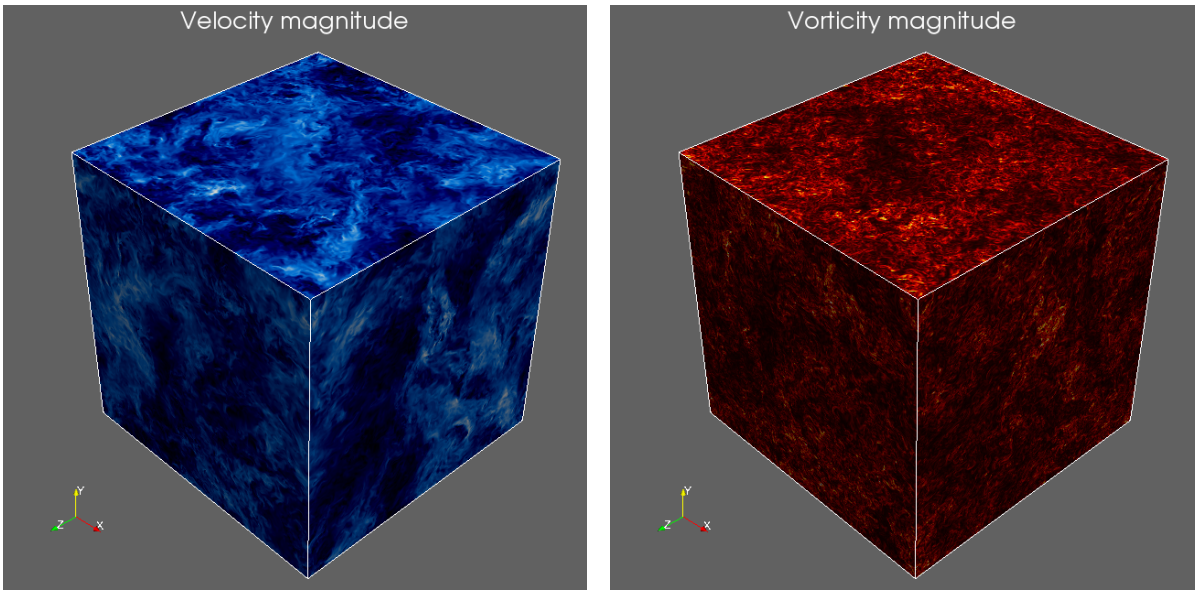

Figure 4.2: Velocity (left) and vorticity (right) magnitude visualisation for JHTD dataset flow. Higher magnitudes are represented by a lighter colour, lower magnitudes by a darker colour.

5

METHODOLOGY

5.1. EDDIES AS REGIONS OF HIGHLY COHERENT MOTION

In daily life, eddies are recognized easily: the water draining out of your bathtub, a smoke ring, or a tornado are obvious examples which anyone could identify as swirling flows. Recognizing an eddy in isotropic turbulence presents a greater challenge, since the scales lie much closer together than they do in a tornado. There exists no precise mathematical definition of an eddy. For the purposes of this research, an eddy will be defined as a finite region of the flow displaying a certain coherent structure, which will generally be swirling or vortex-like. Since the flows under consideration are all isotropic, there is no mean flow to be considered — the flow is statistically similar in all directions.

5.1.1. DEFINING THE CORRELATION FUNCTIONS

REGIONS OF HIGH VELOCITY CORRELATION

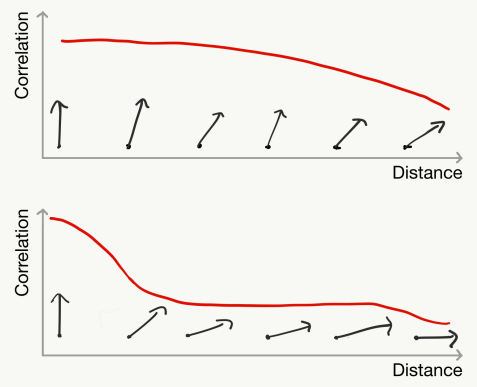

Figure 5.1

The objective is to define a function, taking as input a velocity field, and yielding a value for each point quantifying the correlation of the flow around that point. An obvious starting point is the inner product: vectors that are inline with each other, and vectors that are opposite each other, will have a large (absolute) inner product, whereas vectors that are closer to being perpendicular will have a very small inner product. Consider a point $\mathbf{x}_1$ having a velocity $\mathbf{u}(\mathbf{x}_1)$, and another point $\mathbf{x}_2$, having velocity $\mathbf{u}(\mathbf{x}_2)$. If these points are part of a swirling eddy, their velocities should correlate to some extent; for example, if the points lie in line with the 'eye' of the eddy, their velocity vectors can be expected to be roughly parallel. If $\mathbf{x}_1$ is indeed part of an eddy, the inner product of $\mathbf{x}_1$ and any point in a straight line from it through the eddy should be large. This motivates considering the correlation function as the sum of inner products in a straight line from a given point, normalized by the maximum value. The correlation function is thus defined as:

$$f(\mathbf{x},\mathbf{e}) = \int_{-\infty}^{\infty} \frac{\mathbf{u}(\mathbf{x})\cdot\mathbf{u}(\mathbf{x}+\mathbf{e}r)}{\max(|\mathbf{u}(\mathbf{x})\cdot\mathbf{u}(\mathbf{x}+\mathbf{e}r)|)}\,dr, \tag{5.1}$$

where $\mathbf{e}$ is a unit vector in the direction along which the correlation is being calculated.

An illustrative example of how this correlation function operates is helpful. Consider the vectors in figure 5.1. Assume the correlation is being calculated for the leftmost point, and directed along the x-axis. The vectors in the top graph are aligned well with this leftmost vector, which means the inner products will be large, and hence the integral over these inner products will be large. The vectors in the bottom graph, however, are almost perpendicular to the leftmost vector and hence the correlation value will be small in this case. For a uniformly random flow field, the correlation everywhere should be uniform (and zero on average) as well. However, if a swirling eddy exists, it will manifest itself as a region of high coherence.

Note that this correlation function definition relies on the isotropy of the flow; if the correlation were calculated for a fluid flowing through a tube, for example, there would be a strong correlation in the direction of the flow everywhere.

REGIONS OF HIGH VORTICITY CORRELATION

In addition to investigating regions of high velocity correlation, it is interesting to consider regions of high vorticity correlation. The result of this is less intuitive; vorticity is hard to imagine, and the characteristics of a turbulent eddy in the vorticity field unknown. It was investigated nonetheless. Simply replacing velocity with vorticity in 5.1 yields.

$$f(\mathbf{x},\mathbf{e}) = \int_{-\infty}^{\infty} \frac{\boldsymbol{\omega}(\mathbf{x}) \cdot \boldsymbol{\omega}(\mathbf{x}+\mathbf{e}r)}{\max(|\boldsymbol{\omega}(\mathbf{x}) \cdot \boldsymbol{\omega}(\mathbf{x}+\mathbf{e}r)|)} dr. \tag{5.2}$$

CORRELATING VORTICITY WITH VELOCITY

Lastly, it makes sense to consider both the velocity and the vorticity field. It is known that a vortex tube generates a circular velocity field around it (see figure 5.2). Thus one might expect that the cross product of the vorticity at the centre of the tube and the velocity outside the tube would be large. This motivates the third correlation function, defined as:

$$f(\mathbf{x},\mathbf{e}) = \int_{-\infty}^{\infty} \frac{\boldsymbol{\omega}(\mathbf{x}) \times \mathbf{u}(\mathbf{x}+\mathbf{e}r)}{\max(|\boldsymbol{\omega}(\mathbf{x}) \times \mathbf{u}(\mathbf{x}+\mathbf{e}r)|)} dr. \tag{5.3}$$

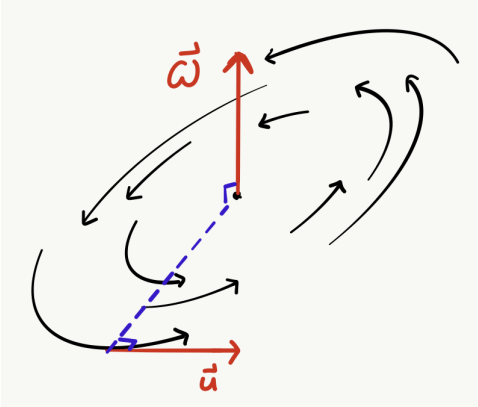

Figure 5.2: The relation between vorticity and velocity; by definition, a point with a large vorticity vector will have a circular flow (following the right hand rule) directly around it. If this circular flow is not limited to just the direct vicinity of the point, but is seen further away from it as well, then it can be considered a turbulent eddy.

5.1.2. APPLYING THE CORRELATION FUNCTIONS

Initially, the correlation functions were applied to Flow A flow directions x, y and z, for a wide range of timesteps. In the preliminary results, coherent regions seemed to form mainly along the principal axes (which will be elaborated upon in chapter 6). To determine the origin of this bias, the correlation functions were applied to flow A along diagonal axes in the xy-plane, the yz-plane and the xz-plane. Additionally, the correlation functions were applied to a single timestep of the JHTD flow. For this report, the directions x, y and z will be referred to as the *principal axes*, and the diagonal directions in the xy-plane, the yz-plane and the xz-plane will be referred to as the *diagonal axes*.

5.2. RECONSTRUCTING THE VELOCITY FIELD FROM AN EDDY

Once coherent regions of high correlation have been found, the focus can be shifted to the flow they produce and their evolution over time. The goal is to visualize the velocity field that a coherent region generates. As mentioned before, the Biot-Savart law can be applied to a vorticity field to retrieve its associated velocity field:

$$\mathbf{u}(\mathbf{x}) = \frac{1}{4\pi} \int_V \frac{\boldsymbol{\omega}(\mathbf{x}') \times \mathbf{r}}{|\mathbf{r}|^3} d\mathbf{x}', \qquad \mathbf{r} = \mathbf{x} - \mathbf{x}'. \tag{5.4}$$

Thus the velocity at a point $\mathbf{x}$ consists of contributions from the vorticities of all points within the domain. The effect of the contribution diminishes rapidly with the distance from $\mathbf{x}$ due to the denominator $|\mathbf{r}|^3$.

For the purpose of this project, it is not the entire velocity field which is of interest, but solely the part generated by a coherent blob. To implement this, the vorticity field is masked; all vorticities outside the blob are set to zero, while the vorticity inside the blob is retained. Thus a velocity field is found for the entire domain, solely from the vorticity inside the blob. Effectively, the velocity field is being spatially filtered to retain only the structure associated with the blob.

6

RESULTS AND DISCUSSION

For reference purposes, table 6.1 gives an overview of the correlation functions and the basic way in which they operate.

6.1. RESULTS OF APPLYING THE CORRELATION FUNCTIONS

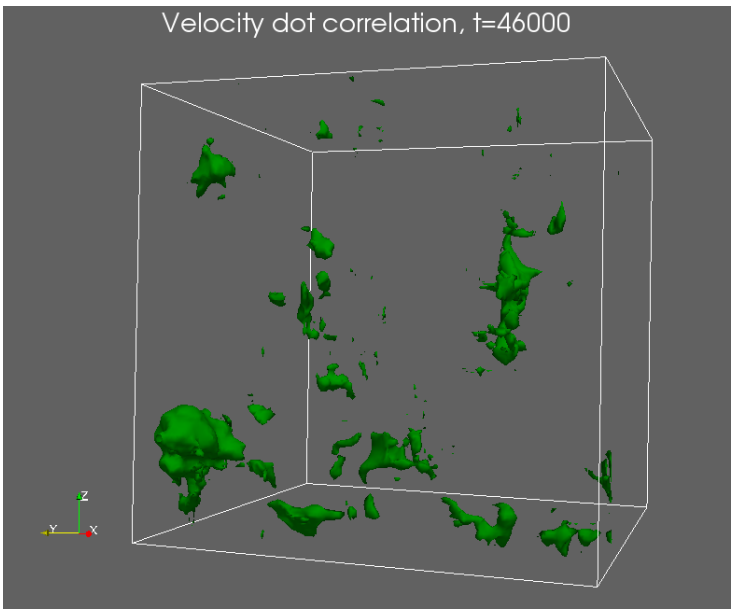

Figure 6.1: Velocity correlation for flow A at t=46000. Isosurface at 70% of maximum.

Figure 6.1 displays the correlation field resulting from a single timestep of flow A. In this case, the velocity correlation function has been applied. The blobs that can be seen are isosurfaces within which the correlation magnitude is greater than 70% of the maximum correlation. These blobs are an indication of coherent structures in the flow.

Some clarification about the terminology relating to the structures is useful here. The goal is to find and visualize **eddies**, defined as coherent structures within the velocity field. An isosurface in 6.1 can be considered as the **kernel** of an eddy. Figure 6.2 illustrates the relationship between an eddy in the velocity field and a kernel of the correlation field. The kernel is indicative of a larger coherent structure. The values of the correlation field within this kernel are related to the size of the eddy. The dimensions of the kernel are assumed to yield less information about the size of the associated eddy, since they are a result of the choice of isosurface. In this report, the terms 'blob' and 'kernel' will be used somewhat interchangeable when referring to an isosurface in the correlation field, whereas an eddy is used to refer to a coherent structure in the velocity field.

When viewing multiple timesteps in sequence, the blobs can be seen appearing, moving, merging, splitting up and disappearing, which would be expected of eddies as well. If the isosurface is taken at a higher

Function name	Correlation by
Velocity correlation	$\mathbf{u}(\mathbf{x}) \cdot \mathbf{u}(\mathbf{x}+\mathbf{r})$
Vorticity correlation	$\boldsymbol{\omega}(\mathbf{x}) \cdot \boldsymbol{\omega}(\mathbf{x}+\mathbf{r})$
Vorticity/velocity cross correlation	$\boldsymbol{\omega}(\mathbf{x}) \times \mathbf{u}(\mathbf{x}+\mathbf{r})$

Table 6.1: An overview of the free correlation functions, and the value each function calculates.

value, smaller structures within the blobs can be seen. If the isosurface is taken at lower values, larger structures are observed.

Figure 6.3 displays the breaking of one blob into two smaller blobs. It is tempting to consider this as an eddy breaking into two smaller eddies. One problem with this is that the smaller kernels still have the same correlation value as the larger one, which disagrees with the theory of eddies of a large scale breaking into eddies of a smaller scale. In fact, it is difficult at the moment to say much about the scale of the coherent structure at all. For now, all that can be said is that a single coherent region has split into two distinct coherent regions with the same correlation value.

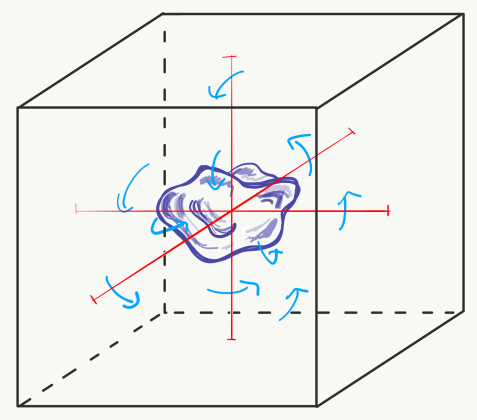

Figure 6.2: An isosurface in the correlation field indicates the presence of a larger structure surrounding it.

The vorticity correlation function and the vorticity/velocity cross correlation function were also applied to the flow. Figures 6.6(a,b,c) display the three correlation functions applied along the principal axes for flow A. In the velocity correlation field and the vorticity/velocity cross correlation field, distinct kernels can be seen, although the blobs for the vorticity/velocity cross correlation are somewhat more patchy.

The correlation field resulting from the vorticity correlation (figure 6.6(b)) is somewhat less clear: the blobs are very patchy, and seem to be biased towards the principal axes, along which the correlation is calculated. The bias may be inherent to the way the correlation is being calculated — by calculating along a certain set of axes, contributions to structures which are aligned along those axes are magnified. The reason this bias is observed so strongly in the vorticity correlation may be that vorticity is associated with the smaller scales, thus giving a smaller correlation value over long distances. Following this line of reasoning, the magnitude of the correlation vectors in the velocity correlation and the vorticity/velocity correlation is relatively larger, and the contribution of directional bias is small, due to which it does not appear when taking the isosurface. In the vorticity correlation function, the correlation field is small everywhere, and directional bias contributions are larger compared to true coherent structure contributions.

Another hypothesis for the origin of the directional bias is that it is inherent to the forcing scheme employed, which forces in the principal directions. To investigate whether or not this is the case, the three functions were applied along the diagonal axes as well, the results of which are displayed in figures 6.6(d,e,f). Here there appears to be a bias towards the diagonal directions along which the correlation is calculated, which negates the hypothesis.

At first glance, the six fields pictured in figure 6.6 don't seem to resemble each other very much. However, there are some similarities; in many timesteps, the correlation fields resulting from the velocity correlation and those resulting from the vorticity/velocity cross correlation show similarities in structure and location of blobs. The vorticity correlation field seems to impart little knowledge about the structure and location of blobs.

The three correlation functions were applied to the JHTD flow as well, both along the principal axes (fig-

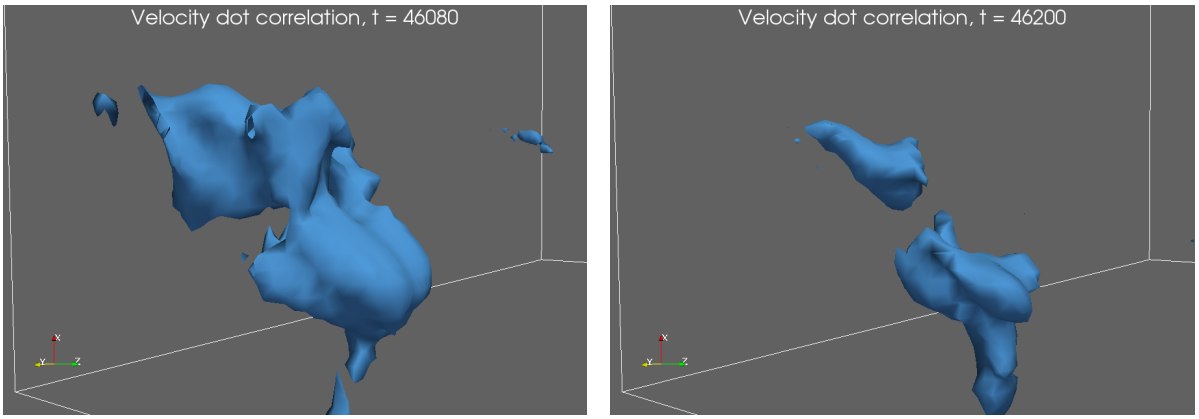

Figure 6.3: A coherent region breaking up. Isosurface at value 120 (roughly 90% of the maximum value), t= 46080,46200. The blobs have a characteristic size of roughly 20 dimensionless length units

ures 6.7(a,b,c)) and along diagonal axes (figures 6.7(d,e,f)). The results are very similar to those of flow A. For example, directional bias is observed more strongly when the correlation is calculated along the principal axes than when it is calculated along diagonal axes. The vorticity correlation field once again shows less coherent structures, to the extent that the correlation field is not far from homogeneous, and shows the strongest directional bias. In the vorticity correlation field it is also made clear that the directional bias is inherent to the correlation method, and not due to the forcing scheme, since the bias is equally present in figures 6.7(b) and 6.7(c).

One way in which the JHTD correlation fields differ from the flow A correlation fields, is that the isosurfaces appear to be less smooth. This may be due to the fact that JHTD has a larger resolution. It could also be due to the fact that the dataset was coarse-grained from 1024^3 to 512^3 gridpoints.

The similarity between the velocity correlation field and the vorticity/velocity correlation field is clearly visible in the JHTD flow. Figure 6.4 displays a superposition of those two fields, calculated along diagonal axes. The vorticity/velocity cross correlation field is by definition assumed to show mainly swirling structures. The fact that it is strongly similar to the velocity correlation field, which should show correlation of any structure, lends support to the idea that coherent structures in isotropic turbulence are swirling or vortex-like in nature.

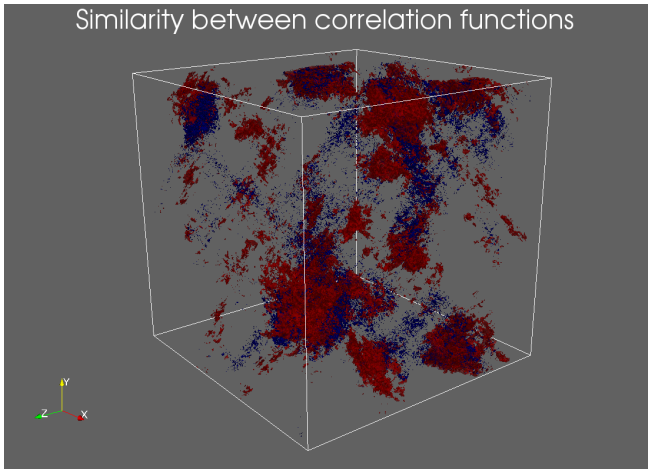

Figure 6.4: Velocity dot correlation (red) and vorticity-velocity cross correlation (blue) calculated diagonally for the JHTD flow. The coherent regions are found in approximately the same locations in the domain.

Earlier attempts at locating turbulent eddies focused on areas of high kinetic energy in a spectrally filtered velocity field. For comparative purposes, this method was applied to a single timestep of the velocity field from flow A. The field was transformed to Fourier space. Wavenumbers between $k = 1$ and $k = 5$ (i.e. the large scale structures) were retained, wavenumbers outside the range were filtered out. After transforming the field back to real space, isosurfaces of high kinetic energy were visualized. Figure 6.5 displays a comparison between the results of the spectral filtering method and the velocity correlation function.

The results of the spectral filtering method are smoother than those of the correlation function, which is to be expected since larger wavenumbers (associated with smaller structures) have been filtered out. The general shapes of the blobs are similar to the blobs found using the correlation formulae. For this timestep, it is difficult to conclude much about a relationship between the location of structures in one field with those in the other. Some blobs do appear in roughly the same location, for example the elongated structure on the left hand side of the figure, but others appear only in one of either fields.

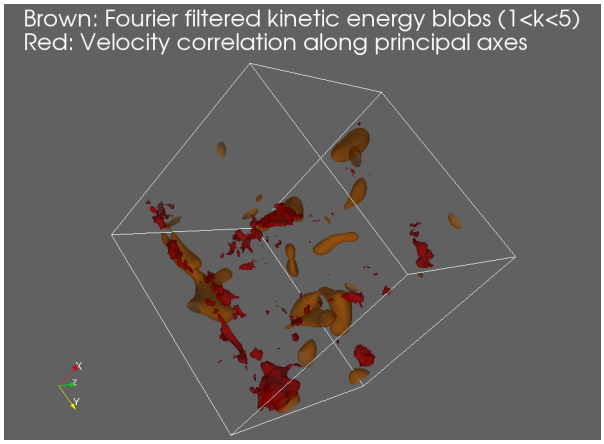

Figure 6.5: Comparison between eddy identification using spectral filtering with kinetic energy isosurfaces and eddy identification using the velocity correlation function, both at ~80% of the maximum value.

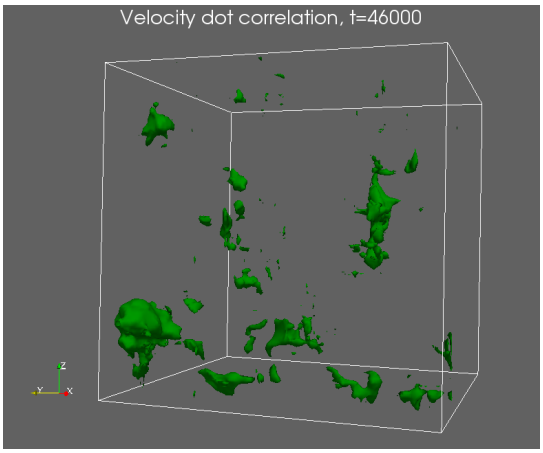

(a) Velocity correlation at 70% of maximum

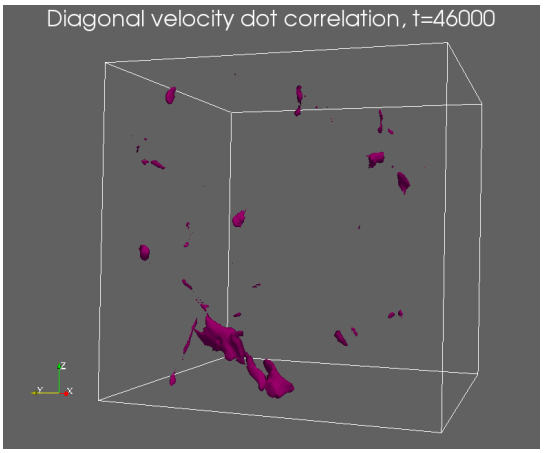

(d) Diagonal velocity correlation at 80% of maximum

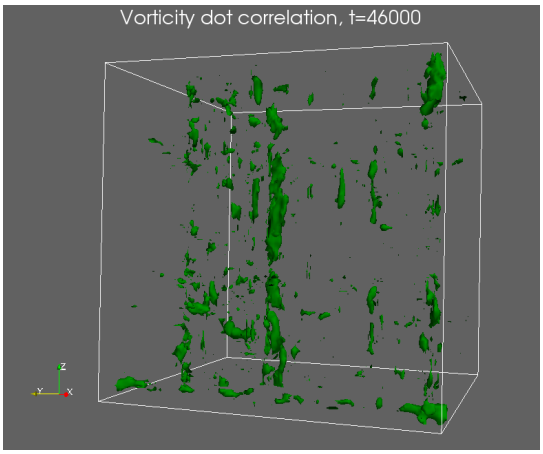

(b) Vorticity correlation at 70% of maximum

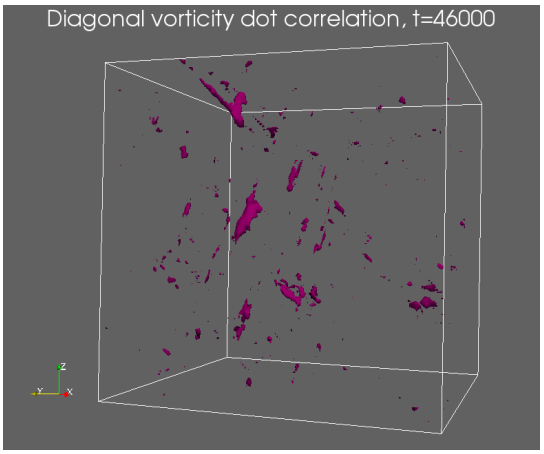

(e) Diagonal vorticity correlation at 60% of maximum

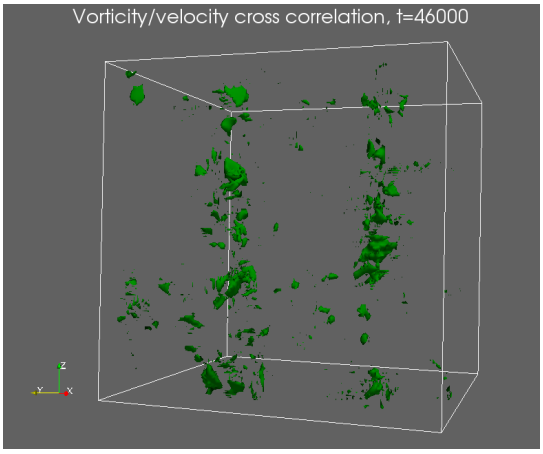

(c) Vorticity/velocity cross correlation at 70% of maximum

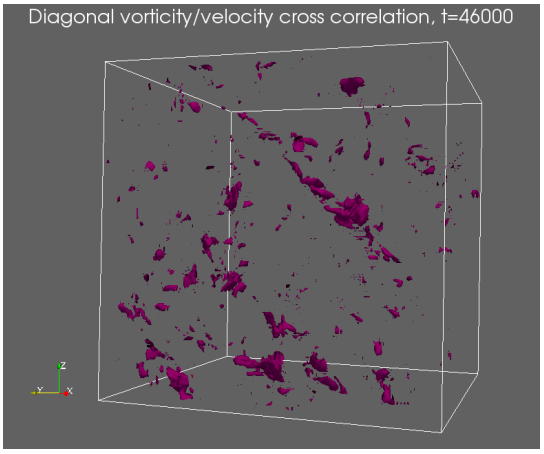

(f) Diagonal vorticity/velocity cross correlation at 70% of maximum

Figure 6.6: The three correlation functions applied to flow A at t=46000. Left: Along principal axes. Right: Along diagonal axes.

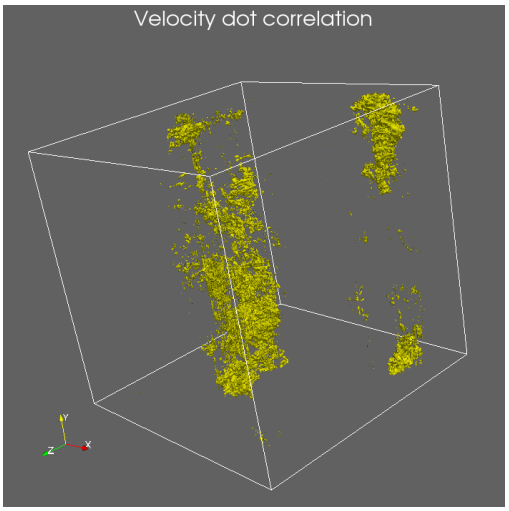

(a) Velocity correlation at 80% of maximum

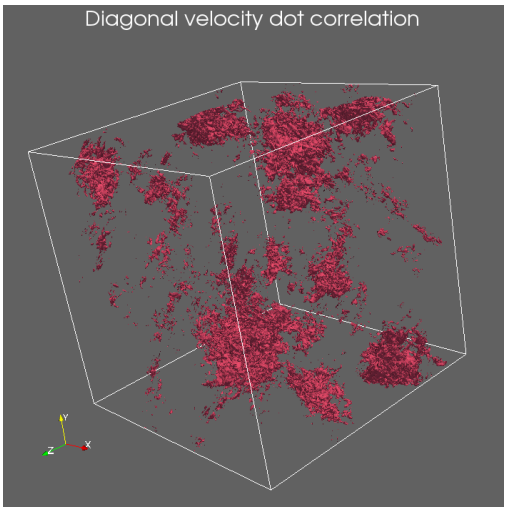

(d) Diagonal velocity correlation at 70% of maximum

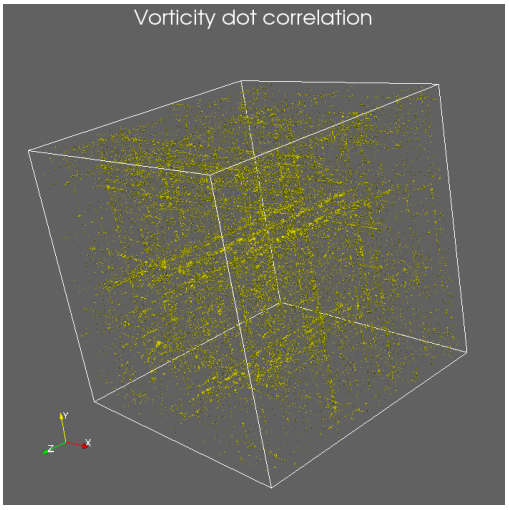

(b) Vorticity correlation at 50% of maximum

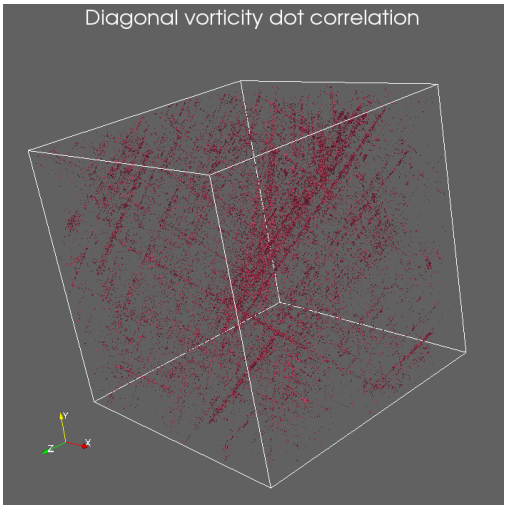

(e) Diagonal vorticity correlation at 50% of maximum

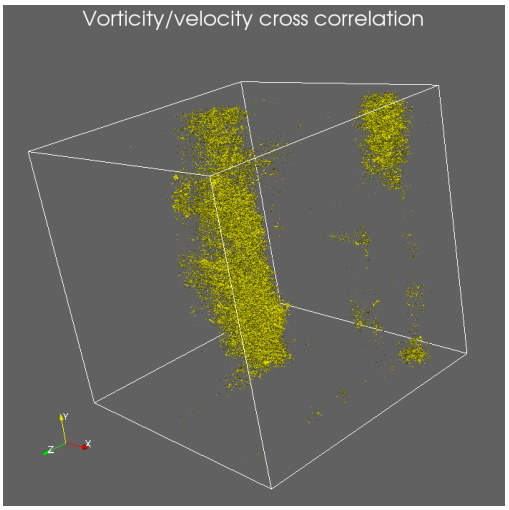

(c) Vorticity/velocity cross correlation at 65% of maximum

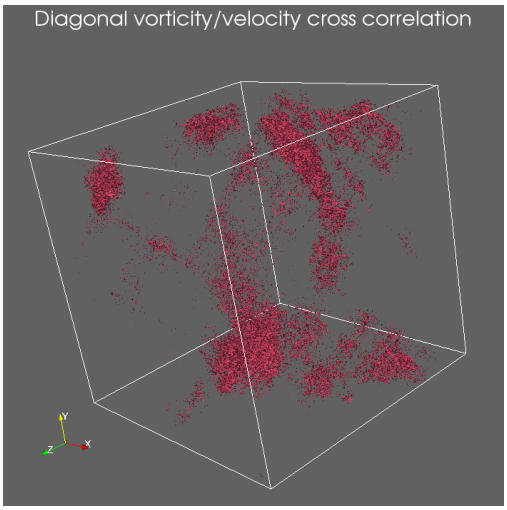

(f) Diagonal vorticity/velocity cross correlation at 70% of maximum

Figure 6.7: The three correlation functions applied to the JHTD flow. Left: along principal axes. Right: along diagonal axes.

6.2. RESULTANT VELOCITY FIELDS

The second research goal is to visualize the velocity field associated with the blobs resulting from the correlation functions. A consecutive series of timesteps from flow A in which a coherent kernel is seen breaking into two separate kernels was selected. The Biot-Savart law can be used to generate the velocity field associated with just the kernel by masking the vorticities outside of it.

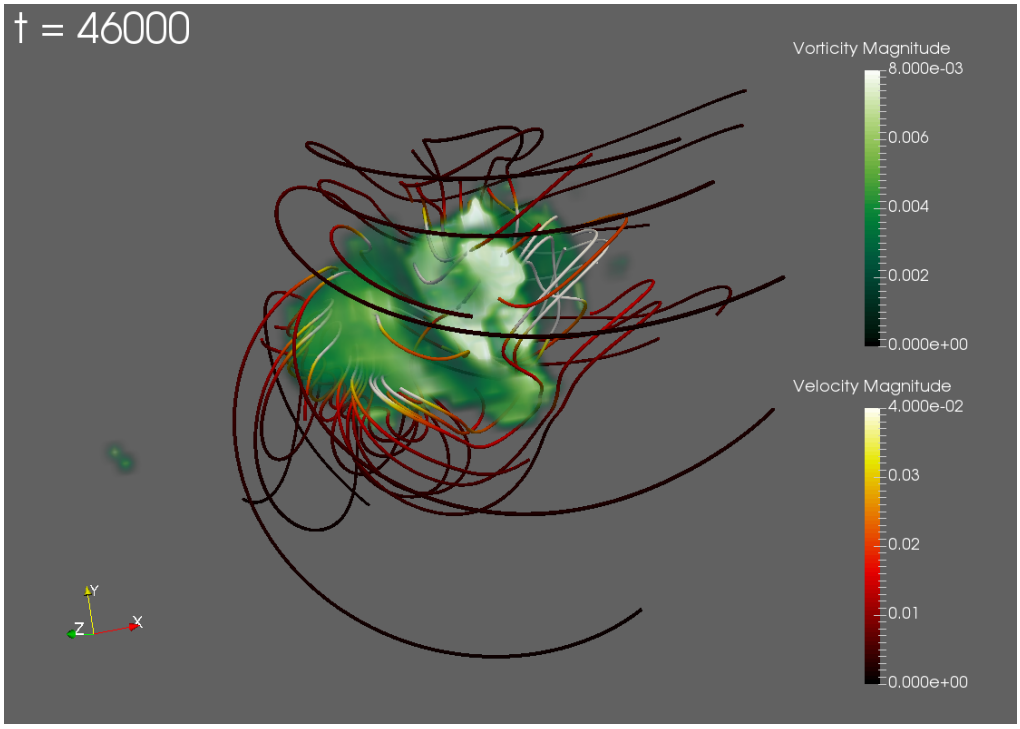

Figure 6.8: The velocity field generated from a coherent blob found using the velocity correlation function, and the coherent blob itself.

Figure 6.8 displays the resultant velocity field of a kernel in the velocity correlation field[7] at $t = 46000$. The kernel has a characteristic size of roughly 20 dimensionless length units, or 15% of the domain size.

The velocity field is represented by streamlines coloured according to the velocity magnitude, with low velocity in dark red and high velocity light yellow. The vorticity field is represented by a volume render, with low vorticity in dark green and high vorticity in light green. As expected, the blob forms the kernel of a coherent structure in the space around it. The velocities close to and inside of the blob are high compared to those far from it, which is also to be expected, since the denominator in the Biot-Savart law increases rapidly with distance.

When velocity streamlines are taken over the whole field, the finer structure is lost, and all that remains is a large swirling vortex with very low velocity. This implies that the effect of a blob is noticeable mainly in the region close to it. The structure of the streamlines close to the kernel shows a complex swirling pattern. This is better illustrated by plotting solely the streamlines, which is done in figure 6.9. There seem to be three vortex-like structures: (i) a large scale, low-velocity vortex around the entire kernel, (ii) a tight, high-velocity vortex on the left-hand side of the kernel, and (iii) a tight, high-velocity vortex behind the kernel. The large scale vortex does not contribute much to the velocity field of the flow, but the development of two tight vortices near the boundary is interesting — perhaps these structures are being formed by the main coherent structure and will develop into smaller separate coherent structures eventually.

The velocity field was generated in the same manner for a range of consecutive timesteps. During this range, the blob breaks into two distinct blobs. At $t = 46120$, the breaking up has occurred. Figures 6.10 and 6.11 display the resulting velocity field.

Once again, the velocity is highest at short distances from the blob, and decays rapidly with distance. The two main blobs seem to have distinct vortices associated with them, which may be evolutions of the distinct tight vortices seen in figure 6.9. This could be the visualization of an eddy breaking into two smaller eddies.

[7] The choice for a blob from the velocity correlation field, as opposed to the vorticity/velocity cross correlation field, is somewhat arbitrary. As was seen in chapter 6.1, the fields are very similar.

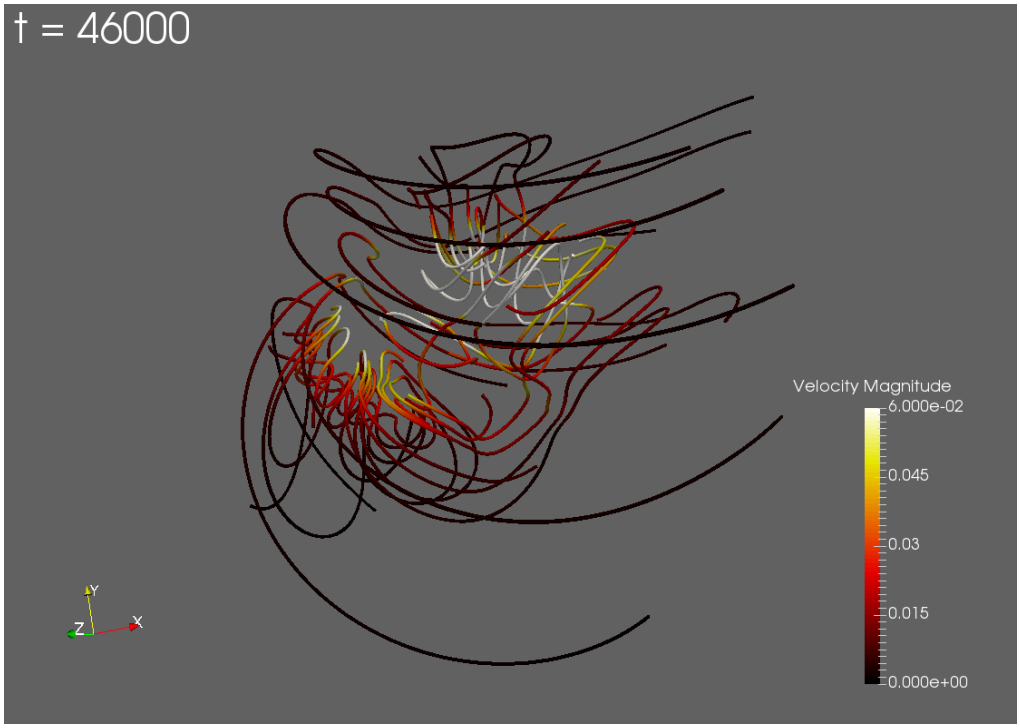

Figure 6.9: The velocity field generated from the same coherent blob as in figure 6.8

However, it must be noted that the two kernels have the same correlation isosurface value. If the correlation value is linked to the scale of an eddy, it would be expected that when an eddy breaks, new kernels are formed at a smaller correlation scale. Since no formal attempt at linking correlation to scale has been made yet, all that can be said at the moment is that in this case, a kernel breaking into two kernels seems to generate two separate vortices.

Figures 6.12 and 6.13 display the same blobs, with their associated velocity profile, some timesteps later at $t = 46280$. The blobs have diminished in size, and the vorticity profile has lost some of its defining features, turning into a rather simple vortex. The distinct vortex-like structures from the previous timesteps are not seen anymore.

Figures 6.14 and 6.15 display the full time evolution of the blob and its associated velocity field. From these figures, it is hard to draw a definite conclusion about what happens to the distinct vortex-like structures seen in 6.9 and 6.10. One possibility is that they have merged back into the main vortex, which would imply that what was observed was not a vortex breaking up at all. Another possibility is that they have been fully separated from the original structure, and are not anymore generated by the vorticity inside the coherent blobs, but are instead their own separate coherent structures.

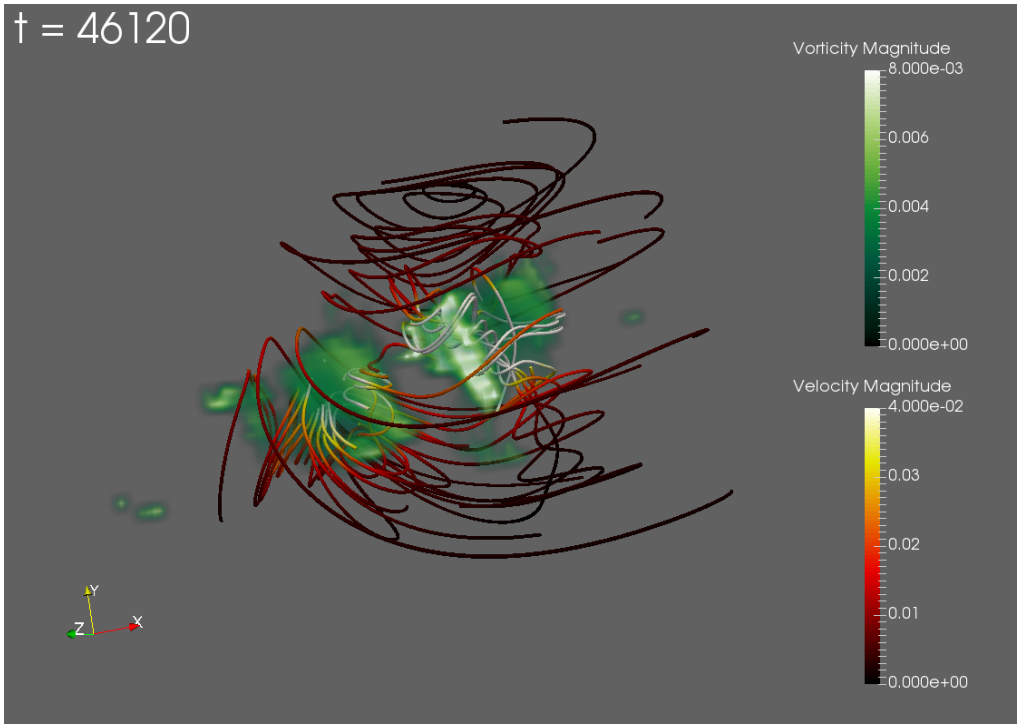

Figure 6.10: The blob, now split up into two separate blobs, and the velocity field they generate at t=46120

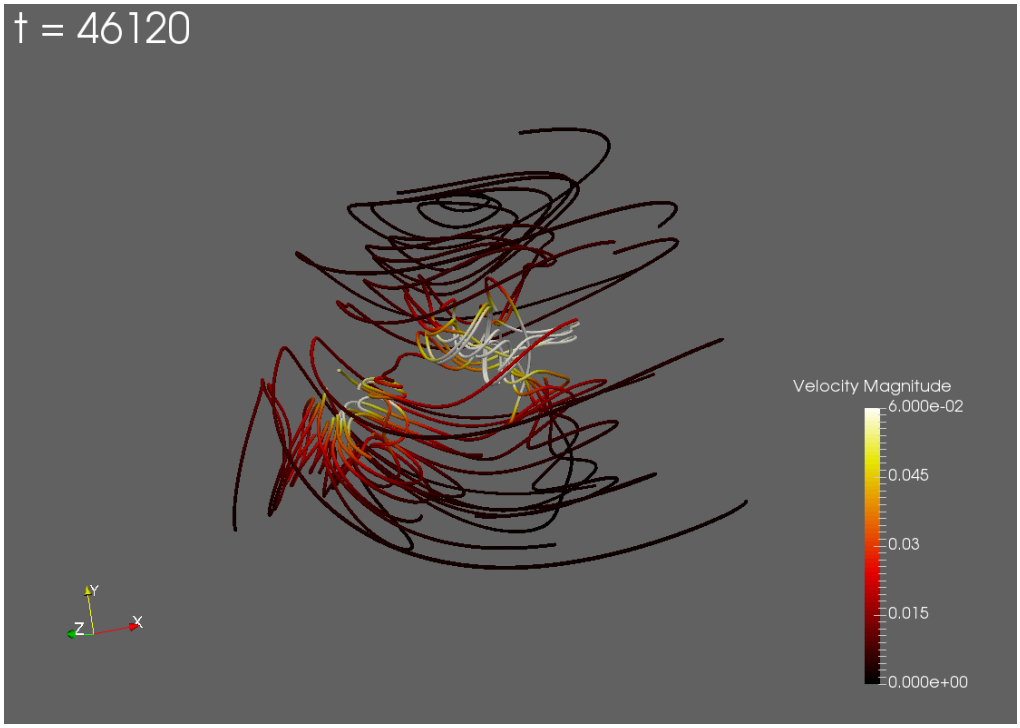

Figure 6.11: The streamlines associated with the kernel at t=46120

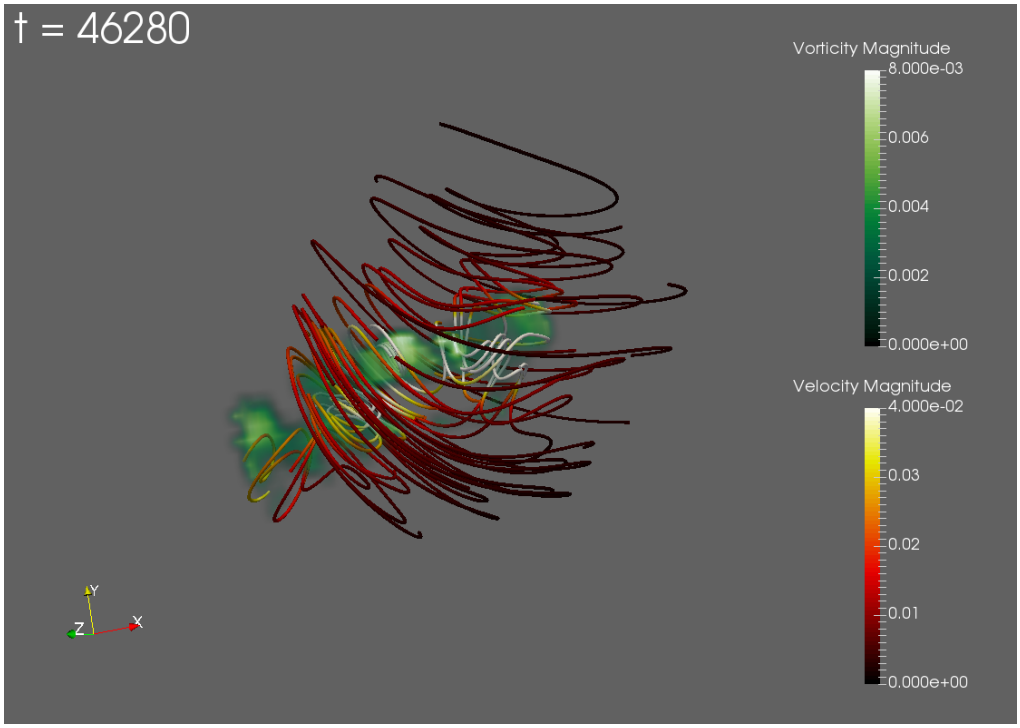

Figure 6.12: The blobs and the velocity field they generate at t=46280

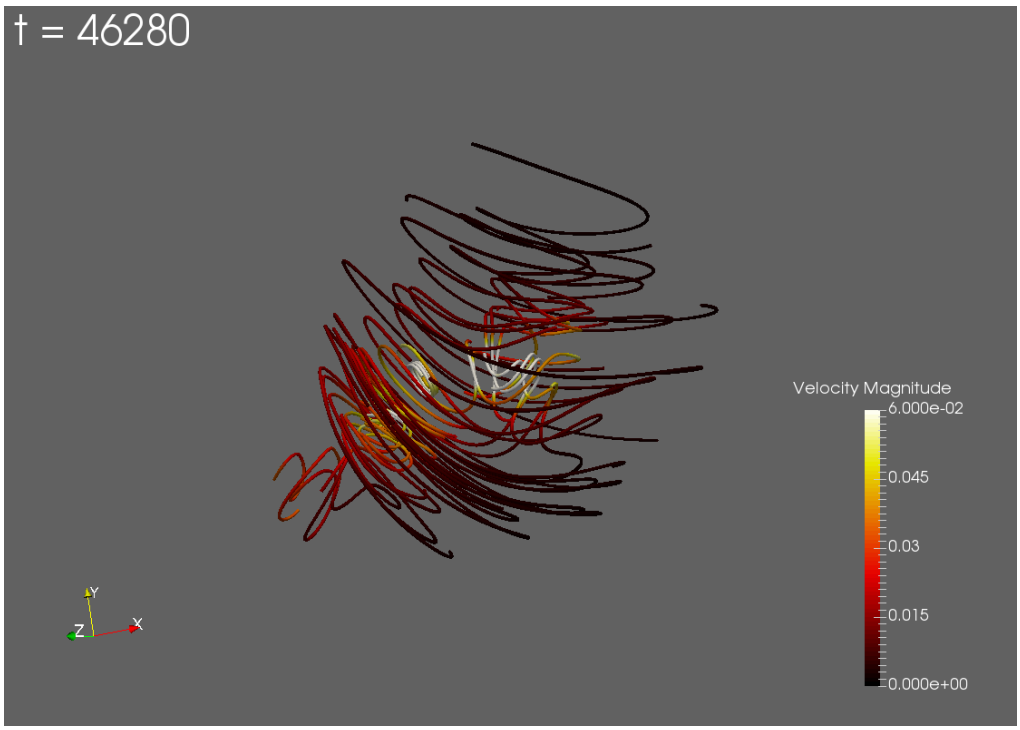

Figure 6.13: The streamlines associated with the kernel at t=46280

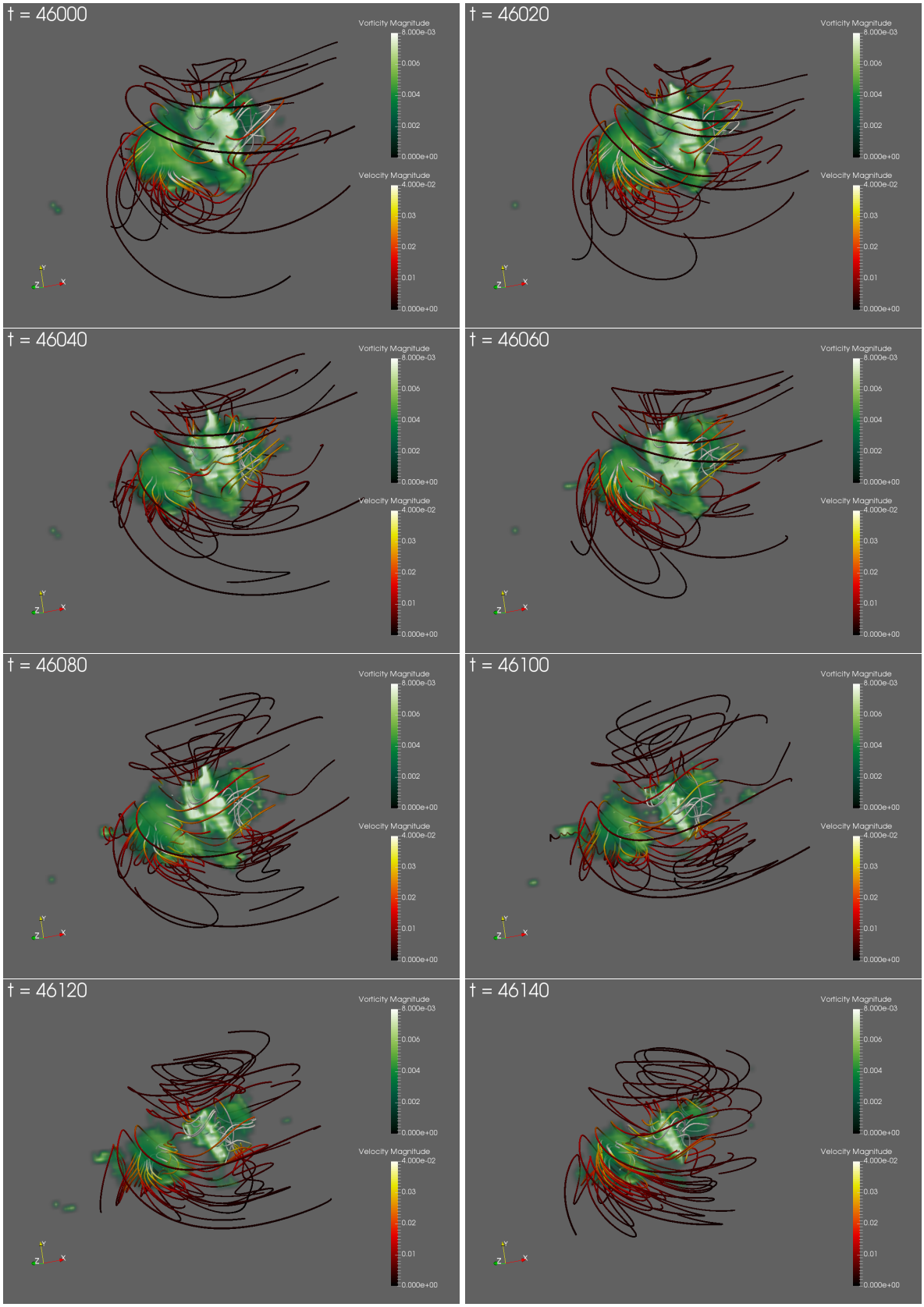

Figure 6.14: Reconstructing a velocity field from a coherent blob of vorticity.

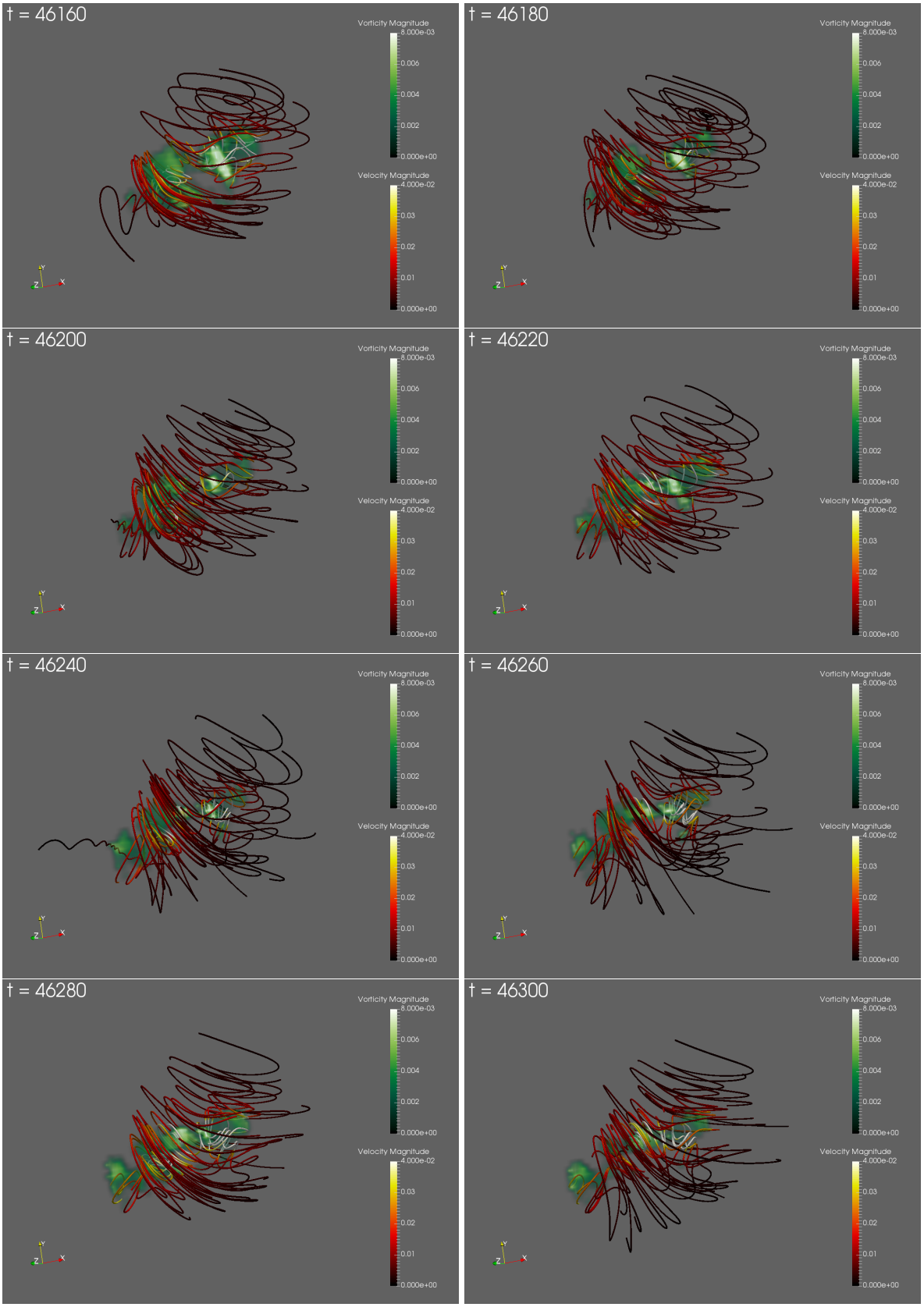

Figure 6.15: Reconstructing a velocity field from a coherent blob of vorticity.

7

CONCLUSION

The long-term goal of the research started during this project is to visualize the turbulent energy cascade. To make headway with this grand aspiration, two smaller short-term questions were proposed. These are to determine how *(i)* eddies can be described as regions of highly coherent motion in turbulent flow, and to determine how *(ii)* the velocity fields associated with these eddies can be visualized.

To answer the first question, several novel correlation functions were introduced. Two of these functions show promising results. These are the velocity dot correlation and the vorticity/velocity cross correlation. In contrast to earlier attempts to visualize turbulent eddies, these functions are not restricted to local values, and take into account structure as well as magnitude of the coherent region. The resultant correlation fields display regions of high correlation, which can be seen as kernels of larger coherent structures.

There is a directional bias in the location of kernels, which tend to appear as elongated structures in the direction along which the correlation was calculated. This directional bias is most clearly observed in the vorticity correlation field. This field is nearly homogeneous, with a grid-like arrangement of blobs. This directional bias appears to be inherent to the correlation functions. The reason the bias appears so prominently in the vorticity correlation field may be that there is less large scale correlation in the vorticity field, and thus the bias-effect begin to dominate over the effect of true correlation.

The fields resulting from the velocity correlation function and the vorticity/velocity cross correlation function display similarities with each other. This reinforces the idea that turbulent eddies are swirling or vortex-like.

In the correlation field resulting from the velocity correlation function and the correlation field resulting from the vorticity/velocity cross correlation function, the kernels can be seen splitting up over time. This could be an indication of a large coherent structure separating into two coherent structures. The scale of the structure, however, is related to the correlation value in the kernel. Since the two resultant kernels have the same correlation value, it can not yet be said whether the splitting implies energy being transferred across scales.

A correlation field resulting from the velocity correlation function has been compared to a spectrally filtered velocity field. It was found that there did appear to be some overlap in the location of the correlation kernels and the location of the filtered kinetic energy isosurfaces. If this overlap is a chance occurrence, or if it appears systematically, has not been investigated yet.

The velocity correlation field has been used to answer the second research question. Biot-Savart's law can be used to generate the velocity field associated with a vorticity field. In Biot-Savart's law, the velocity at a point consists of contributions from the vorticity of all points in the domain. To visualize the velocity field associated with only the kernel of a correlation field, the vorticity outside the kernel was set to zero. In this way, the velocity field consisting only of contributions from inside the kernel can be generated.

This was done for several consecutive timesteps in which a single kernel separates into two distinct kernels. It was found that a kernel generates a velocity field in the entire domain, although the velocities far from the kernel are very small. When viewed from a distance, the velocity field appears to be a simple vortex-like structure surrounding the kernel. However, when the velocity field close to the kernel is investigated, complex structures appear.

The velocity field resulting from the specific kernel investigated for this project displayed two distinct tight vortex-like structures at the boundaries of the kernel. Over time, these structures grow further apart,

as the kernel separates into two kernels. This might be a visualization of the eddy break-up mechanism in action. Some timesteps later, the distinct structures seem to have disappeared, and the general structure of the velocity field around the kernel becomes simple again. Possibly, the structures disappear because they are no longer associated with this kernel, but are now the result of two separate kernels on a smaller scale.

With more investigation into the correlation kernels of smaller-scale structures, it may be possible to follow a coherent structure down the entire turbulent energy cascade. In any case, the results of this project are promising, and the author is hopeful that they will lead to a better understanding of the turbulent energy cascade in the future.

8

RECOMMENDATIONS FOR FURTHER RESEARCH

This project has served as an initial probe into a methodology which may shed more light on the mechanisms of the turbulent energy cascade. As it stands now, there still does not exist a strict description of an eddy, its break-up mechanism, or its relation to the turbulent energy cascade. If such a description exists and can be found by continuing down the path started upon in this project, the following challenges should be addressed:

RELATING STRUCTURES TO SCALES

In order to arrive at a visualization of the turbulent energy cascade, eddies at many scales must be identified and visualized. The kernels in the correlation fields found in this research are probably associated with the larger scales of the turbulent energy cascade, but their exact 'wavenumber' is not defined. Relating the blobs to their place in the cascade could elucidate the process of energy transfer through scales. To do this, it would be necessary to find kernels at the smaller scales as well.

Perhaps this is possible by making use of Fourier filtering. This could be approached in two ways. The velocity field could be spectrally filtered to retain only a certain range of wavelengths, from which the correlation field can be calculated. Another approach is to spectrally filter the *correlation field*. Since the correlation field is a vector field, the large scale structures can be filtered out, after which an isosurface can be constructed from the resultant field after inverse Fourier transformation. The benefit of the latter approach over the former is its cheaper computational cost. Calculating the correlation field is expensive, whereas spectral filtering is relatively cheap. However, it is not yet clear what a filtered correlation field would mean physically.

FINETUNING THE CORRELATION FUNCTION

As it is defined now, the correlation function shows a bias towards blobs arranged along the axes upon which the correlation is calculated. This makes sense from a mathematical perspective, but not from a physical perspective. A better correlation function might incorporate many more directions, or might correct for directional bias in a different way. This would come at a higher computational cost, but might yield better results.

Another problem which must be overcome occurs when presented with a perfectly symmetrical velocity field. Consider the vector field illustrated in figure 8.1, where the velocity at each point is proportional to the distance of the point from the center of the vortex. If the velocity correlation function is applied to this field at point $\mathbf{x}_1$, the resultant correlation will be zero, since the positive contributions of all the points to the left of the center are cancelled by the negative contributions of all the points to the right of the center. If the correlation function is applied to the field close at $\mathbf{x}_2$, the resultant correlation will be zero as well, since there is no velocity at $\mathbf{x}_2$, so all inner products will be zero[8].

The solution to the first problem may be to integrate over the absolute values of the inner product. A solution to the second problem might be to disregard the point itself, but correlate by the points directly around it. In any case, these problems requires some attention.

[8] Technically, the correlation result at point $\mathbf{x}_2$ will even be undefined, since the denominator will be zero as well.

SYSTEMATIC DEFINITION OF A CORRELATION KERNEL

The kernels identified in this project were chosen by hand, with little to no system concerning the correlation value at which the isosurfaces were made. For results that are reproducible, comparable and useful for other research as well, some work must be done towards a systematic definition of a kernel.

STATISTICAL ANALYSIS OF THE SIMILARITIES BETWEEN FUNCTIONS

Three correlation functions have been defined and applied, of which two showed similar blob locations and structure. In addition, the similarity to the earlier method of spectral filtering has been compared. The amount of similarity between between these correlation functions, as well as the similarity between principal and diagonal axes of correlation, should be investigated further. This may shed more light on the different aspects of isotropic turbulence each function reveals in its correlation field.

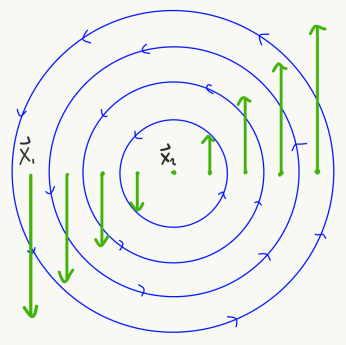

Figure 8.1: A perfectly symmetrical rigid body vortex, in which $u \propto r$, where r is the distance from the center of the vortex.

A

DERIVATION AND EXPLANATION OF RELEVANT EQUATIONS

A.1. THE CONTINUITY EQUATION

Consider a small differential control volume within a flowing fluid (with density ρ). Setting up a mass balance over this control volume yields

$$\frac{dm}{dt} = \dot{m}_{in} - \dot{m}_{out}, \tag{A.1}$$

since mass can neither be created nor destroyed. The terms in A.1 can be rewritten to yield

$$\frac{dm}{dt} = dx\,dy\,dz\,\frac{d\rho}{dt} \tag{A.2}$$

$$\begin{aligned}\dot{m}_{in} &= \dot{m}|_{x=x}\,dy\,dz + \dot{m}|_{y=y}\,dx\,dz + \dot{m}|_{z=z}\,dx\,dy \\ &= \rho\,u_x|_{x=x}\,dy\,dz + \rho\,u_y|_{y=y}\,dx\,dz + \rho\,u_z|_{z=z}\,dx\,dy\end{aligned} \tag{A.3}$$

$$\begin{aligned}\dot{m}_{out} &= \dot{m}|_{x=x+dx}\,dy\,dz + \dot{m}|_{y=y+dy}\,dx\,dz + \dot{m}|_{z=z+dz}\,dx\,dy \\ &= \rho\,u_x|_{x=x+dx}\,dy\,dz + \rho\,u_y|_{y=y+dy}\,dx\,dz + \rho\,u_z|_{z=z+dz}\,dx\,dy.\end{aligned} \tag{A.4}$$

Thus we find, after some rearrangement,

$$\frac{d\rho}{dt} = \frac{\rho\,u_x|_{x=x} - \rho\,u_x|_{x=x+dx}}{dx} + \frac{\rho\,u_y|_{y=y} - \rho\,u_y|_{y=y+dy}}{dy} + \frac{\rho\,u_z|_{z=z} - \rho\,u_z|_{z=z+dz}}{dz}. \tag{A.5}$$

Taking the limit of the differential lengths to zero finally yields

$$\frac{d\rho}{dt} + \nabla\cdot(\rho\mathbf{u}) = 0. \tag{A.6}$$

This is the continuity equation in its differential form. Since the fluid is incompressible, that is since ρ is constant, A.6 reduces to

$$\nabla\cdot\mathbf{u} = 0. \tag{A.7}$$

A.2. THE NAVIER-STOKES EQUATION

To derive the Navier-Stokes equations, Newton's second law of motion is applied to a small volume of fluid δV:

$$\text{forces acting on } \delta V = \text{mass of } \delta V \cdot \text{acceleration of } \delta V. \tag{A.8}$$

The mass of δV is $\rho\,\delta V$. To calculate the acceleration of δV it must be taken into account that the volume is flowing with the liquid. To describe the rate of change in velocity at each point of the volume's trajectory, first consider the increment in $\mathbf{u}(\mathbf{x}, t)$ for arbitrary and independent increments $d\mathbf{x}$ and dt,

$$d\mathbf{u} = \frac{\partial\mathbf{u}}{\partial t}dt + \frac{\partial\mathbf{u}}{\partial x_i}dx_i. \tag{A.9}$$

Here tensor notation has been used in the second term of the right-hand side, where summation over the repeated index is implied. Now if the increments in space and time are not arbitrary and independent, but instead follow the trajectory of the particle, they can be related to the velocity,

$$dx_i = u_i dt. \tag{A.10}$$

Substitution of A.10 in A.9 yields

$$\frac{D\mathbf{u}}{Dt} = \frac{\partial \mathbf{u}}{\partial t} + u_i \frac{\partial \mathbf{u}}{\partial x_i} = \text{acceleration of } \delta V, \tag{A.11}$$

where the notation using capital D has been introduced to signify the fact that a *material* derivative is being used. Thus the right-hand side of A.8 becomes

$$\rho \delta V \frac{D\mathbf{u}}{Dt}. \tag{A.12}$$

Now, the different forces acting on δV must be described. These are the body forces, i.e. gravity, and the surface forces. Gravity is of course given by $F_g = \rho \delta V \mathbf{g}$. To describe the surface forces, assume that the differential volume is cube-shaped, as in section 2.1. At each surface, we have a normal force, and shear stresses perpendicular to the direction the surface is facing. Consider the forces working in the x-direction first; the derivation of the forces working in the y- and z-direction is completely analogous.

On the surfaces of the cube perpendicular to the flow, there is a normal stress σ_{xx}, while on the surfaces parallel to the flow there is a shear stress τ_{yx} and τ_{zx}. Evaluating these surface forces at the respective surfaces and rewriting yields

$$\begin{aligned}
\Sigma F_x &= \text{gravity in x-direction} + \text{surface forces in x-direction} \\
&= \rho g_x dx dy dz + (\sigma_{xx}|_{x+dx} - \sigma_{xx}|_x) dy dz + \\
&\quad (\tau_{yx}|_{y+dy} - \tau_{yx}|_y) dx dz + (\tau_{zx}|_{z+dz} - \tau_{zx}|_z) dx dy \\
\frac{\Sigma F_x}{\delta V} &= \rho g_x + \frac{d\sigma_{xx}}{dx} + \frac{d\tau_{yx}}{dy} + \frac{d\tau_{zx}}{dz}.
\end{aligned} \tag{A.13}$$

To relate A.13 to the viscosity and fluid velocity, use the constitutive equations

$$\sigma_{xx} = -p + 2\mu \frac{\partial u_x}{\partial x} \tag{A.14}$$

$$\tau_{x_i x_j} = \mu \left(\frac{\partial u_i}{\partial x_j} + \frac{\partial u_j}{\partial x_i} \right). \tag{A.15}$$

Substituting these relations in A.13 yields, after some rewriting,

$$\frac{\Sigma F_x}{\delta V} = \rho g_x - \frac{dp}{dx} + \mu \left(\frac{\partial^2 u_x}{\partial x^2} + \frac{\partial^2 u_x}{\partial y^2} + \frac{\partial^2 u_x}{\partial z^2} \right) + \mu \frac{\partial}{\partial x} \left(\frac{\partial u_x}{\partial x} + \frac{\partial u_y}{\partial y} + \frac{\partial u_z}{\partial z} \right). \tag{A.16}$$

Since the fluid is incompressible, the second term on the right-hand side is equal to zero, and we are left with

$$\frac{\Sigma F_x}{\delta V} = \rho g_x - \frac{dp}{dx} + \mu \left(\frac{\partial^2 u_x}{\partial x^2} + \frac{\partial^2 u_x}{\partial y^2} + \frac{\partial^2 u_x}{\partial z^2} \right). \tag{A.17}$$

Now the sum of forces acting on the differential cube is known, and equating that with A.12 (from which the differential volume δV can be divided out) leads to the Navier-Stokes equation in the x-direction:

$$\rho g_x - \frac{dp}{dx} + \mu \left(\frac{\partial^2 u_x}{\partial x^2} + \frac{\partial^2 u_x}{\partial y^2} + \frac{\partial^2 u_x}{\partial z^2} \right) = \rho \frac{Du_x}{Dt}. \tag{A.18}$$

Analogously, the Navier-Stokes equations in the y- and z-direction can be derived, and combining these three yields, after some rewriting:

$$\frac{D\mathbf{u}}{Dt} = \mathbf{g} - \nabla \left(\frac{p}{\rho} \right) + \nu \nabla^2 \mathbf{u}. \tag{A.19}$$

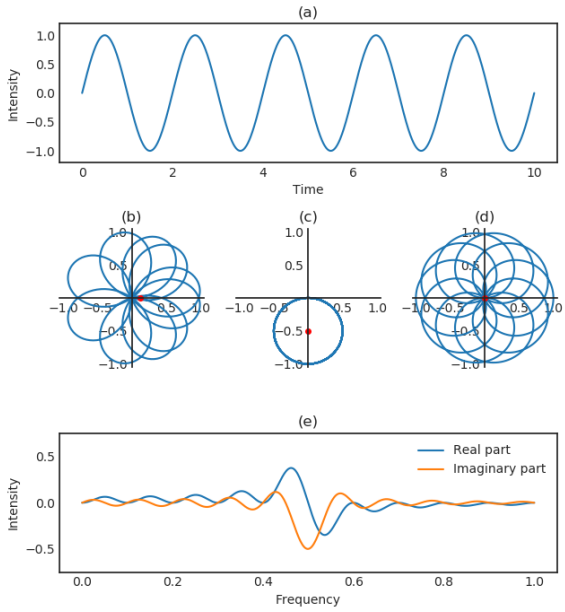

Figure A.1: (a) The original function, $g(t) = \sin 2\pi \cdot 0.5t$. (b) $g(t) \cdot \exp(-2\pi i \cdot 0.35t)$ on the complex plane. (c) $g(t) \cdot \exp(-2\pi i \cdot 0.5t)$, where the centre of mass is clearly shifted. (d) $g(t) \cdot \exp(-2\pi i \cdot 0.6t)$. (e) The location of the centre of mass for a range of frequencies, i.e. the 'intensity' of the centre of mass.

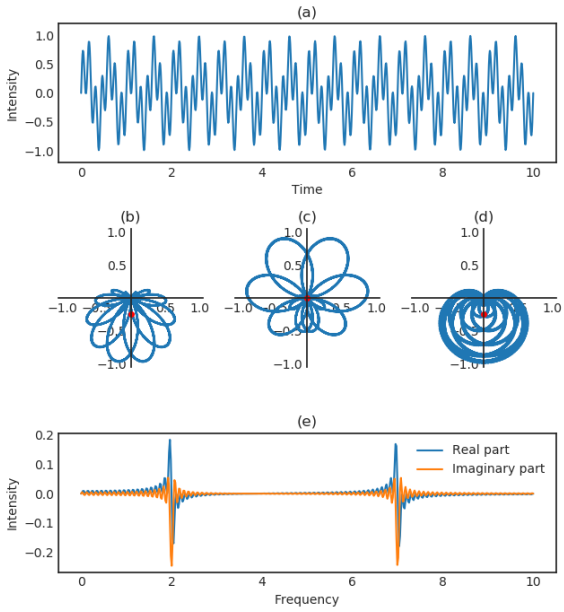

Figure A.2: (a) The original function, $g(t) = 0.5 \cdot (\sin 2\pi \cdot 2t + \sin 2\pi \cdot 7t)$. (b,c,d) 'Wrapped' in the complex plane, using wrapping frequencies 2,3 and 7 respectively. (e) The location of the centre of mass for a range of frequencies, i.e. the 'intensity' of the centre of mass.

A.3. THE FOURIER TRANSFORM

In analyzing the isotropic turbulence, a convenient way of isolating the parts of the flow corresponding to certain wavenumbers or frequencies is desirable. To do this, the Fourier transform is used.

Consider the function $g(t) = \sin 2\pi \cdot 0.5t$, a pure sine wave with frequency 0.5 (figure A.1a). This might represent the air pressure next to a speaker producing a tone with frequency 0.5. The idea behind the Fourier transform is to wrap the output of this function for a certain time-interval around the origin. A convenient way to achieve this is to use Euler's formula, $\exp -2\pi i t\zeta$, where ζ is the wrapping frequency. This is done in figures A.1b, A.1c and A.1d. The centre of mass is represented by a red dot.

The interesting thing to note here is that the location of the centre of mass in the complex plane is dependent on the wrapping frequency ζ. Generally, the positive and negative amplitudes in the sine wave cancel out, and the centre of mass wobbles around the origin. However, when the wrapping frequency coincides with the signal frequency, all the peaks and valleys of the original signal line up, and the centre of mass shifts significantly. In figure A.1e, the real and imaginary parts of the location of the centre of mass are plotted for a range of wrapping frequencies. As expected, they wobble about zero, only deviating when the wrapping frequency coincides with the signal frequency.

Now consider a signal consisting of two frequencies, $g(t) = 0.5 \cdot (\sin 2\pi \cdot 2t + \sin 2\pi \cdot 7t)$ (figure A.2a). Once again wrapping it for several wrapping frequencies (figures A.2b, A.2c and A.2d), and plotting the location of the centre of mass for different frequencies (figure A.2e), two distinct peaks are found corresponding to the frequencies making up the original signal.

This forms the basis of the Fourier transform. One notable difference between the functions plotted in figures A.1e and A.2e and the actual Fourier Transform of their respective inputs, is that the Fourier transform does not normalize the centre of mass, thus a signal which persists for a longer period of time will be more prominently visible in the Fourier transform.

By flattening peaks for certain wavenumbers in Fourier space, and subsequently transforming the signal back to real space using the inverse Fourier transform, the part of the original field corresponding to those wavenumbers can be eliminated. In this way it is possible to isolate only the parts of the field associated with a certain range of wavenumbers.

BIBLIOGRAPHY

[1] A. N. Kolmogorov, *The local structure of turbulence in incompressible viscous fluid for very large reynolds numbers,* in *Dokl. Akad. Nauk SSSR*, Vol. 30-4 (1941) pp. 299–303.

[2] J. Jiménez, A. Vela-Martín, and J. I. Cardesa, *The turbulent cascade in five dimensions,* Science , eaan7933 (2017).

[3] C. Dana Lynn, *Hearth and campfire influences on arterial blood pressure: Defraying the costs of the social brain through fireside relaxation,* Evolutionary Psychology **12**, 147470491401200509 (2014).

[4] P. W. Wiessner, *Embers of society: Firelight talk among the ju'hoansi bushmen,* Proceedings of the National Academy of Sciences **111**, 14027 (2014).

[5] J. Hunt, N. Sandham, J. Vassilicos, B. Launder, P. Monkewitz, and G. Hewitt, *Developments in turbulence research: a review based on the 1999 programme of the isaac newton institute, cambridge,* Journal of Fluid Mechanics **436**, 353 (2001).

[6] P. Kundu and I. Cohen, *Fluid Mechanics* (Elsevier Academic Press, 2002).

[7] P. Davidson, *Turbulence: an introduction for scientists and engineers* (Oxford University Press, USA, 2004).

[8] R. Panton, *Incompressible Flow* (Wiley, 2013).

[9] M. Lesieur, *Turbulence in Fluids* (Springer, 1997).

[10] B. B. Mandelbrot, *Intermittent turbulence in self-similar cascades: divergence of high moments and dimension of the carrier,* Journal of Fluid Mechanics **62**, 331 (1974).

[11] K. Sreenivasan and C. Meneveau, *The fractal facets of turbulence,* Journal of Fluid Mechanics **173**, 357 (1986).

[12] G. I. Taylor, *Statistical theory of turbulence,* Proceedings of the Royal Society of London. Series A, Mathematical and Physical Sciences **151**, 421 (1935).

[13] W. Heisenberg, *On the theory of statistical and isotropic turbulence,* Proc. R. Soc. Lond. A **195**, 402 (1948).

[14] C. v. Weizsäcker, *Das spektrum der turbulenz bei großen reynoldsschen zahlen,* Zeitschrift für Physik **124**, 614 (1948).

[15] L. Onsager, *Statistical hydrodynamics,* Il Nuovo Cimento (1943-1954) **6**, 279 (1949).

[16] C. Meneveau and T. S. Lund, *On the lagrangian nature of the turbulence energy cascade,* Physics of Fluids **6**, 2820 (1994).

[17] S. A. Orszag, *Analytical theories of turbulence,* Journal of Fluid Mechanics **41**, 363 (1970).

[18] R. P. Feynman, *Perfectly reasonable deviations from the beaten track: The letters of Richard P. Feynman* (Basic Books, 2008).

[19] K. Alvelius, *Random forcing of three-dimensional homogeneous turbulence,* Physics of Fluids **11**, 1880 (1999).

[20] A. ten Cate, E. van Vliet, J. Derksen, and H. V. den Akker, *Application of spectral forcing in lattice-boltzmann simulations of homogeneous turbulence,* Computers & Fluids **35**, 1239 (2006).

[21] P. Perlekar, L. Biferale, M. Sbragaglia, S. Srivastava, and F. Toschi, *Droplet size distribution in homogeneous isotropic turbulence,* Physics of Fluids **24**, 065101 (2012).

[22] John Hopkins Turbulence Databases, *Forced isotropic data set,* (2017).